

Lawrence Berkeley National Laboratory

LBL Publications

Title

THEORY OF STATIC STRUCTURAL PROPERTIES, CRYSTAL STABILITY, AND PHASE TRANSFORMATIONS: APPLICATION TO Si AND Ge

Permalink

<https://escholarship.org/uc/item/7vw2s1wp>

Authors

Yin, M.T.
Cohen, M.L.

Publication Date

1982-03-01



Lawrence Berkeley Laboratory

UNIVERSITY OF CALIFORNIA

RECEIVED
LAWRENCE
BERKELEY LABORATORY

FEB 9 1983

LIBRARY AND
DOCUMENTS SECTION

Materials & Molecular Research Division

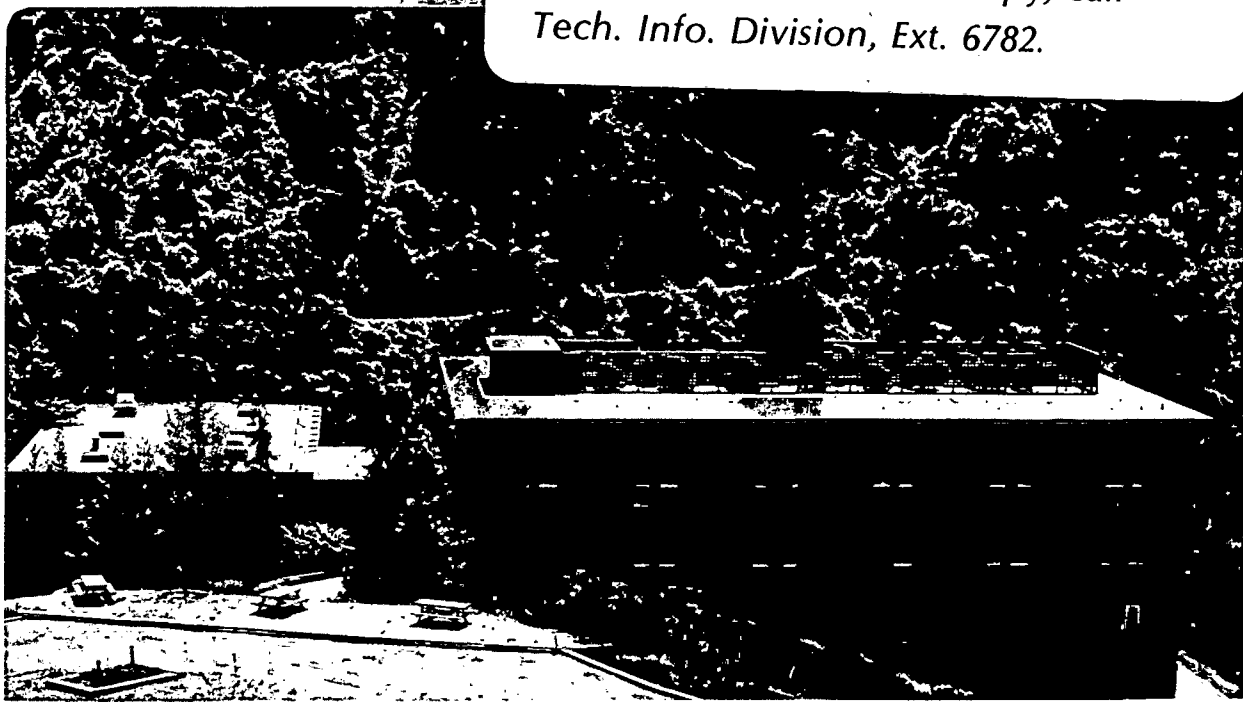
Submitted to Physical Review B

THEORY OF STATIC STRUCTURAL PROPERTIES, CRYSTAL
STABILITY, AND PHASE TRANSFORMATIONS: APPLICATION
TO Si AND Ge

M.T. Yin and Marvin L. Cohen

March 1982

TWO-WEEK LOAN COPY
*This is a Library Circulating Copy
which may be borrowed for two weeks.
For a personal retention copy, call
Tech. Info. Division, Ext. 6782.*



LBL-14835
e.2

DISCLAIMER

This document was prepared as an account of work sponsored by the United States Government. While this document is believed to contain correct information, neither the United States Government nor any agency thereof, nor the Regents of the University of California, nor any of their employees, makes any warranty, express or implied, or assumes any legal responsibility for the accuracy, completeness, or usefulness of any information, apparatus, product, or process disclosed, or represents that its use would not infringe privately owned rights. Reference herein to any specific commercial product, process, or service by its trade name, trademark, manufacturer, or otherwise, does not necessarily constitute or imply its endorsement, recommendation, or favoring by the United States Government or any agency thereof, or the Regents of the University of California. The views and opinions of authors expressed herein do not necessarily state or reflect those of the United States Government or any agency thereof or the Regents of the University of California.

Theory of Static Structural Properties, Crystal Stability,
and Phase Transformations: Application to Si and Ge

M. T. Yin[†] and Marvin L. Cohen

Department of Physics, University of California, and
Materials and Molecular Research Division, Lawrence
Berkeley Laboratory, Berkeley, California 94720

Abstract

We demonstrate that not only the static structural properties but also the crystal stability and pressure-induced phase transformations in solids can be accurately described employing an ab initio pseudopotential method within the local density-functional formalism. Using atomic numbers of constituent elements and a subset of crystal structures as the only input information, the calculated structural properties of Si and Ge are in excellent agreement with experiment.

I. INTRODUCTION

In this paper, we present an ab initio microscopic study of the static structural properties and other important structural properties including crystal stability and phase transformation of Si and Ge. Part of the results have been previously reported.¹ The method is based on a pseudopotential approach and uses the local density-functional approximation² which has also been used in all-electron calculations of static structural studies of metals.³

We choose Si and Ge as our prototypes since they are the most studied semiconductors experimentally. Both have the (cubic) diamond structure and are found to undergo a semiconductor-metal phase transformation under pressure.⁴ Using the x-ray diffraction technique, the transformed phases have been determined⁵ to be of the tetragonal β -tin form. These structural transformations are accompanied by a large volume decrease⁵ (22.7% for Si and 20.7% for Ge). Because of the difficulty in accurate pressure calibration, there has been some scattering of the data for the transition pressures.⁶ The transition pressures were first measured⁴ to be 150 kbar for Si and 105 kbar for Ge. The more recent values are 125 kbar for Si^{7,8} and 100 kbar for Ge.⁹

In addition to the diamond and β -tin phases, a hexagonal diamond phase has been made¹⁰ for Si at room temperature and atmospheric pressure using a sequence of high-pressure and high-temperature treatments. This phase is semiconducting and has the same density as the (cubic) diamond phase. The

axial ratio is 1.65, very close to the ideal value of 1.633. Since this form has not been found in nature and no large crystals have been prepared,¹⁰ it is metastable with respect to the diamond phase. A similar structural form has not been found in Ge. There are other metastable phases of Si and Ge (a bcc form with 16 atoms per unit cell for Si¹⁰ and Ge¹¹ and a tetragonal form with 12 atoms per unit cell for Ge¹²); these will not be considered in the present study.

There are interesting relations between the general phase transformation in semiconductors and other crystalline properties. Jamieson has related⁵ the transition pressure (P_t) and the atomic volume change (ΔV) in the phase transformation to the fundamental energy gap (E_g), and he obtained an empirical rule of $P_t \Delta V = E_g/2$ for Group IV elements and iso-row III-V compounds. Although this rule is less accurate when later refined experimental data is considered, the trend is still correct. This is consistent with the physical picture that the bigger the energy gap is, the more stabilized the structure is. Phillips¹³ has suggested that ionicity may be an important parameter in characterizing the phase transformation. He noted that the rocksalt structure becomes more favorable as the high-pressure phase with increasing ionicity. The covalent counterpart of the rocksalt structure, that is, the simple cubic structure, is included in the present study.

Pressure-induced phase transformations in tetrahedrally coordinated semiconductors have previously been studied using information from electronic structures. Van Vechten observed¹⁴

that the difference in total energy between the semiconducting diamond phase and the metallic β -tin phase is approximately equal to 1/8 of the difference of the band structure energies between the free-electron gas and the Penn model¹⁵ evaluated at the experimental transition volume of the diamond phase. This, however, can only be regarded as an empirical relation. If accurate eigenvalues obtained from self-consistent band structure calculations are used for the band structure energies, the aforementioned relation no longer holds. A perturbative pseudopotential theory has been used¹⁶ to calculate the thermodynamic parameters involved in the phase transformation. While good agreement with experiment was found in this approach, the error in energy incurred in the perturbative treatment especially when applied to the covalent phase may be of the order of the energy differences involved in the phase transformations (about a few tenths of an eV per atom). Besides, the theory introduced a potential parameter which is adjusted to fit the zero-pressure experimental volume. The sensitive dependence of the theory on that parameter is illustrated in a recent study¹⁷ on the pressure-induced phase transformation of ZnSe using a self-consistent pseudopotential theory. Without adjustment of the potential parameter, the rocksalt structure of ZnSe is calculated to be more stable than the zincblende structure in contradiction to the experimental observation. The theoretical results become consistent with experiment only after the parameter is adjusted to fit the experimental zero-pressure value.

In the following sections, we will first briefly discuss

the ab initio pseudopotential approach¹⁸ to the total energy calculations (Sec. II). The procedures for pseudopotential construction and total energy calculation are described in Sec. III. The results for Si and Ge, which will include (a) static structural properties, (b) crystal stability, (c) pressure-induced phase transformation, and (d) electronic structures, are presented and compared with experiment in Sec. IV. Final conclusions are given in Sec. V. We examine the accuracies of the calculated quantities with regard to various approximations used in the calculation in the appendices.

II. THEORY

In the present study, we use the ab initio pseudopotential approach¹ within the local-density-functional formalism.² This approach has been shown¹⁹ to reproduce all-electron results faithfully. By focusing attention on the valence electrons which play a dominant role in the determination of structural properties, we are spared the computation of core states.

A plane wave basis set is used to represent the (pseudo) valence wavefunctions. Such a basis set describes the charge density in the valence region to the same degree of accuracy for different crystal structures. In other words, the basis is not biased toward a particular crystal structure which is usually difficult to achieve in other choices of basis sets. Furthermore, the angular dependence of the charge density is well accounted for, and there is no need for a spherical averaging procedure of the charge density which may introduce appreciable error in describing highly directional covalent bonds.

The structural properties of solids are studied primarily through comparisons of total energies of systems under investigation. It is advantageous to perform the total energy calculations in momentum space.²⁰ The total energy is given by

$$E_{\text{tot}} = E_{\text{kin}} + E'_{\text{ec}} + E'_H + E_{\text{xc}}[\rho] + E'_{\text{cc}} \quad (1)$$

The individual contributions can be interpreted as: the electronic kinetic energy, the electron-core interaction energy, the electron-electron Coulomb energy, the electronic exchange and correlation energy, and the core-core Coulomb energy (the Ewald energy) respectively. Since the effect of core electrons are included in the pseudopotentials, the term "electrons" used in this paper refers to the valence electrons only. The prime in the second, third, and fifth terms on the right-hand side of Eq. (1) denotes that these terms are reduced finite quantities: because of charge neutrality, the infinite contributions arising from the long-range Coulomb interaction cancel with one another and, thus, are excluded from these three terms.²⁰

$E_{\text{xc}}[\rho]$ is a functional of charge density $\rho(\mathbf{r})$. In the local density-functional approximation,

$$E_{\text{xc}}[\rho] = \int \rho(\mathbf{r}) \epsilon_{\text{xc}}(\rho(\mathbf{r})) d\mathbf{r} \quad (2)$$

where $\epsilon_{\text{xc}}(\rho(\mathbf{r}))$ is a function of $\rho(\mathbf{r})$.

The individual terms (per cell) in Eq. (1) are given by:

$$E_{\text{kin}} = \frac{1}{N} \sum_{i, \mathbf{G}} n_i |\psi_i(\mathbf{k}_i + \mathbf{G})|^2 \frac{\hbar^2 |\mathbf{k}_i + \mathbf{G}|^2}{2m} \quad (3)$$

$$E'_{ec} = \frac{1}{N} \sum_{i, G, G'} n_i \psi_i^*(\underline{\lambda}) \psi_i(\underline{\lambda}) \left\{ V_{ps}(\underline{\lambda}) \right. \\ \left. + \delta_{GG'} \frac{1}{\Omega_c} \int_{\infty} \frac{ze^2}{r} dr \right\}, \quad (4)$$

$$E'_H = \frac{\Omega_c}{2} \sum_{G \neq 0} |\rho(G)|^2 \frac{4\pi e^2}{|G|^2}, \quad \text{and} \quad (5)$$

$$E'_{xc} = \frac{\Omega_c}{2} \sum_G \rho^*(G) \epsilon_{xc}(G) \quad (6)$$

$$E'_{cc} = \frac{1}{2} \sum_{s, s'} z_s z_{s'} e^2 \left\{ \frac{4\pi}{\Omega_c} \sum_{G \neq 0} \left[\frac{1}{|G|^2} \cos[G \cdot (\underline{\tau}_s - \underline{\tau}_{s'})] \right. \right. \\ \left. \left. \exp\left(-\frac{|G|^2}{4\eta^2}\right) \right] - \frac{\pi}{\eta^2 \Omega_c} + \sum'_{\underline{\ell}} \left[\frac{\text{erfc}(\eta x)}{x} \right]_{x=|\underline{\ell} + \underline{\tau}_s - \underline{\tau}_{s'}|} \right. \\ \left. - \frac{2\eta}{\sqrt{\pi}} \delta_{ss'} \right\} \quad (7)$$

The symbols n_i , k_i , and ψ_i are respectively the occupation number, the crystal momentum, and the (pseudo) wavefunction in the momentum representation of state i . N is the total number of cells in the system; Ω_c is the cell volume, and $\underline{\ell}$ and \underline{G} are the direct and reciprocal lattice vectors. $Z \equiv \sum_s z_s$, and z_s and $\underline{\tau}_s$ are the core charge and the position vector for the s^{th} atom in the basis. The symbol $\rho(\underline{G})$ is the Fourier transform of the (pseudo) valence charge density, and $V_{ps}(k_i + \underline{G}, k_i + \underline{G}')$ is the Fourier transform of the superposition of core pseudopotentials in momentum representation. The prime in the $\underline{\ell}$ summation in Eq. (7) excludes the $\underline{\ell} = 0$ term when $\underline{\tau}_s = \underline{\tau}_{s'}$, and η is a parameter controlling the convergency of the Ewald summations.²¹

The momentum-space formalism is closely related to the plane wave method for the calculation of electronic structures. The Schrödinger equation used in the plane wave method can

be easily derived variationally from the expression for the total energy in Eqs. (1)-(7). Using the resulting eigenvalues ϵ_i 's, we obtain an alternative expression for the total energy

$$E_{\text{tot}} = \frac{1}{N} \sum_i n_i \epsilon_i - E'_H + \Delta E_{\text{xc}} + E'_{\text{cc}} \quad (8)$$

where

$$\Delta E_{\text{xc}} = \Omega_c \sum_{\tilde{G}} \rho^*(\tilde{G}) [\epsilon_{\text{xc}}(\tilde{G}) - v_{\text{xc}}(\tilde{G})] \quad (9)$$

and

$$v_{\text{xc}} = \frac{d(\rho \epsilon_{\text{xc}})}{d\rho} \quad (10)$$

The double summation over \tilde{G} 's in Eq. (4) is absorbed in the simple summation of the eigenvalues of the occupied states.

III. CALCULATIONS

A. PSEUDOPOTENTIAL CONSTRUCTION

The ab initio pseudopotentials of Si (Ge) are generated through the Hamann-Schlüter-Chiang method²² using the $3s^2 3p^{0.5} 3d^{0.5}$ ($4s^2 4p^{0.5} 4d^{0.5}$) reference configuration. The r_c values (in a.u.) chosen are 1.17, 1.35, and 1.17 (1.17, 1.36, and 1.36) for the s, p, and d components of the pseudopotential of Si (Ge). The reference configuration has a partially filled d orbital for the generation of the d pseudopotential. The nonlocal (angular-momentum-dependent) pseudopotentials of Si and Ge are shown in Fig. 1. The d pseudopotential of Ge is more repulsive than that of Si because the 4d orbital of Ge has one node and is more extended than the 3d orbital of Si. The repulsive d pseudopotential of Ge pushes the d pseudo-orbital away from

the core to simulate this effect. The Wigner interpolation formula²³ for the exchange and correlation energies is used for the present study.

The pseudopotentials thus generated are examined in the atomic limit. They are capable of reproducing the corresponding all-electron excitation energies and eigenvalues to within a few mRy and wavefunctions (outside the core region) to within 1% for atomic configurations over a wide energy range (about 2 Ry) above the atomic ground state. Examples are given in Table I and Fig. 2. Such agreement is a prerequisite for the solid state calculations using the pseudopotential approximation¹⁸ in which the interaction between the valence electrons and the atomic cores is approximated by pseudopotentials.

B. TOTAL ENERGY CALCULATIONS

For the present study, the total energy as a function of volume was calculated for seven crystal structures: the fcc, bcc, hcp, (cubic) diamond (CD), hexagonal diamond (HD), β -tin, and simple cubic (sc) phases. The first four phases encompass 80% of the observed elemental crystal structures. The HD phase is very similar to the CD phase. The β -tin phase is observed as a high-pressure form for Si and Ge. The simple cubic structure is a covalent counterpart of the NaCl structure. The ideal axial ratio ($c/a = \sqrt{8/3}$) is used for hcp and the HD structures. Several c/a ratios are used for the β -tin structure.

For each crystal structure of Si or Ge, we calculate the total energy at six to fifteen different values of atomic volume ranging from 0.55 to 1.13 times the experimental value of

the diamond phase (Ω_{expt}). For each value of atomic volume, the one-electron Schrödinger equation is solved iteratively to self-consistently²⁴ at which point the input and output screening potentials are identical to within 10^{-4} Ry, and E_{tot} is stable to within 10^{-5} Ry. The wavefunctions are expanded in a plane wave basis set with a kinetic energy cutoff (E_{pw}) of 11.5 Ry. Note that E_{pw} is kept constant for different atomic volumes and different crystal structures. In this way, the smallest wave length of the plane waves used in the finite plane wave expansion is approximately the same; namely, the spatial variations of wavefunctions are accounted for to similar accuracy. Furthermore, $\sqrt{E_{\text{pw}}}$ is a measure of the k-space potential cutoff, that is, the extent to which the pseudopotential is sampled in k-space. If E_{pw} is kept constant, the k-space potential cutoff is practically the same for different atomic volumes and different crystal structures. This facilitates meaningful comparisons of total energies.

The number of sampling k points²⁵ used in the Brillouin zone summation of the electronic density and total energy is increased until E_{tot} converges to the desirable accuracy as described below. For both the CD and HD phases, the calculation yields semiconducting systems, and the absence of Fermi surfaces allows fast convergence for E_{tot} with respect to the number of sampling k points. Ten (six) special k points²⁵ in the irreducible Brillouin zone (IBZ) for the CD (HD) phase are sufficient to achieve 0.3 mRy/atom convergence for E_{tot} .

The other five phases are all found to be metallic in

our calculation. A large number of k points are needed to account for the effects of the Fermi surface. The term most sensitive to the finite number of sampling k points in the total energy calculation [Eq. (8)] is the Brillouin zone summation of valence eigenvalues. A few sampling methods have been examined. They are: (i) the linear tetrahedron method²⁶ in which the Brillouin zone is divided into tetrahedra. The eigenvalues are assumed to vary linearly within each tetrahedron, and this enables an analytic integration inside the tetrahedron. (ii) the discrete sampling method in which the Brillouin zone summation is done in a straightforward manner using special k points.²⁵ (iii) the interpolation method in which the eigenvalues of a set of sampling k points are calculated directly from solving the Schrodinger equation, and the eigenvalues of a much larger set of k points are interpolated and used for the Brillouin zone summation. The interpolation can be carried out through a Fourier series expansion of the eigenvalues. We find that the convergence of the total energy with respect to the number of sampling k points is slow using the linear tetrahedral method. The errors come mainly from the linearization assumption. The convergence is faster if the discrete sampling method is used and even faster if the interpolation method is used.

As a numerical example, the convergent errors (in units of Ry/atom) caused by the finite number of sampling k points in the total energy calculation of the fcc phase of Si at atomic volume $0.75 \Omega_{\text{expt}}$ are 0.05 Ry/atom using 20 k points in IBZ

by the linear tetrahedron method and 0.005 Ry/atom and 0.001 Ry/atom using ten k points in IBZ by the discrete sampling method and the interpolation method respectively. The results presented in the following sections are obtained using the discrete sampling method.²⁷ For a convergence of 0.001 Ry/atom in total energy, the number of sampling k points in IBZ are 24, 35, 70, 36, and 60 for the β -tin, sc, bcc, hcp, and fcc phases respectively.

IV. RESULTS

A. STATIC STRUCTURAL PROPERTIES

The static structural properties such as lattice constant, cohesive energy, and bulk modulus can be obtained from the calculated total energies as a function of volume for the observed crystal structure. We have calculated total energies of the cubic diamond structure of Si and Ge for 15 atomic volumes ranging from 0.55 to 1.13 Ω_{expt} . They are then least-squares fitted to Murnaghan's equation of state,²⁸

$$E_{\text{tot}}(V) = \frac{B_0}{B_0'} \left[\frac{(V_0/V)^{B_0'}}{B_0' - 1} + 1 \right] + \text{constant}, \quad (11)$$

where B_0 and B_0' are the bulk modulus and its pressure derivative at the equilibrium volume V_0 . This equation of state has been examined and found to be quite accurate for quite a few crystals under moderate compression.^{28 b} The minimum total energy (E_{min}), the equilibrium lattice constant, and the bulk modulus are readily deduced from the fitted parameters in the equation of state.²⁹ The cohesive energy is then the difference between

the crystal energy which is the sum of E_{\min} and the zero-point vibration energy and the total energy of the isolated pseudoatom with spin-polarization effects³⁰ included.

The calculated lattice constants, cohesive energies, and bulk moduli are compared with experiment^{31,32,33} in Table II. The agreement is very good. These results also compare well with other ab initio calculations.³⁴ There have also been microscopic calculations of the static structural properties of Si (Ref. 35) and Ge [Ref. 35(a)] using pseudopotentials which are empirically fitted to the observed excitation spectra. These results are somewhat sensitive to the fitted pseudopotential, and the comparisons with experiment are not as good as the ab initio results. It is interesting to note that the band structures of ab initio calculations within the local density-functional formalism cannot be used directly to compare with the excitation spectra; for example, the calculated indirect gap of Si is smaller than the experimental gap by a factor of two (see Sec. IV D).

The least-squares fit to the Murnaghan's equation of state has a rms error of about 10^{-4} Ry/atom. Other functional forms of the equation of state such as a polynomial form of the total energy as a function of the lattice constant, the volume, or their reciprocals have also been examined. The equilibrium lattice constant and E_{\min} are rather insensitive to the functional form of the equation of state. The variations are 10^{-3} Å and 10^{-4} Ry/atom respectively. In contrast, the bulk modulus (B_0) has a variation of about 10%, and its pressure derivative (B'_0)

can vary by a factor of two. The calculated values of B'_0 are 3.2 for Si and 3.7 for Ge using Murnaghan equation of state which compares well with the experimental values³³ of 4.2 for Si and 4.6 for Ge in view of the large theoretical uncertainty.

The above results are calculated using a plane wave kinetic energy cutoff E_{pw} of 11.5 Ry except for the cohesive energy to be discussed later. At this E_{pw} , the lattice constants converge to better than 1%, and the cohesive energies and the bulk moduli converge to about 5% (Appendix A). The dependence of the cohesive energy of Si on E_{pw} is shown in Fig. 3. As E_{pw} increases, the variational freedom of the wavefunctions becomes larger which gives rise to a lower total energy and a larger cohesive energy. The cohesive energy converges rapidly when E_{pw} is larger than 10 Ry. The calculated cohesive energies (per atom) for the case $E_{pw} = 11.5$ Ry are 4.67 eV and 4.02 eV for Si and Ge respectively as compared to the almost fully converged values of 4.84 eV and 4.26 eV using $E_{pw} = 20$ Ry (Table II). The differences in cohesive energy between theory and experiment are 0.21 eV for Si and 0.41 eV for Ge. The pseudopotential approximation¹⁸ accounts for errors of the order of 0.05 eV.¹⁹ The remaining portion of the errors seems to come from the local-density-functional approximation² and the functional form of the exchange-correlation energy, especially for the atomic calculations.³⁶ Even with the spin-polarization effect included in the fashion described in Ref. 30 in the atomic calculations, the calculated ionization potentials of atoms differ from the experimental values by a few tenths of an eV.³⁰

Comparison of various energy contributions to the total energy between an isolated atom and a crystalline atom for Si and Ge are given Table ^{III} Λ . The term E_{pot} is the sum of E'_{ec} , E'_{H} , and E'_{cc} [Eq. (15)]. The term E_{spin} is the energy gain resulting from spin polarization of the atom. It is calculated by taking the total energy difference between the spin-polarized and the unpolarized pseudoatoms with the valence configuration $s^2 p^2$ where the form of ^{the} Λ exchange-correlation energy proposed by Gunnarsson and Lundqvist³⁰ is used. The term E_{vib} is the zero-point vibrational energy estimated from measured phonon frequencies.³⁷ As the crystals form, the electrons become localized to form chemical bonds, which gives rise to an increase in electronic kinetic energy (E_{kin}) and decreases in potential energies (E_{xc} and E_{pot}). We note that both E_{xc} and E_{pot} are essential in stabilizing the crystal. In the absence of either one, the crystal would become unstable. The contributions from E_{spin} and E_{vib} tend to favor the isolated atom, but their effects are not dominant.

Shown in Fig. 4 are contour plots of pseudo valence charge densities of Si and Ge in the (110) plane. Because of the norm-conserving property of ab initio pseudopotentials, the pseudo valence charge distributions are expected to faithfully reproduce real valence charge distributions outside the core region, and there is no need for core orthogonalization. The contour plots for Si and Ge look rather similar.³⁸ The contour lines in the bonding region are elongated along the bonding direction, which agrees with the experimental valence charge

density of Si synthesized³⁹ from the x-ray data.⁴⁰

We have calculated the x-ray structural factors of Si and Ge by adding the core structural factors to the valence structural factors obtained in crystalline calculations. The core structural factors are obtained from atomic calculations with the valence configuration of s^2p^2 . They differ from the corresponding results using valence configuration sp^3 by at most 0.006 e/cell, which demonstrates the inertness of the core electrons as the valence configuration changes. A comparison between calculated x-ray structural factors with experiment⁴⁰⁻⁴² for Si and Ge are given in Table^{IV}_^. The agreement is very good. We note that the (222) reflection, which is forbidden in a simple superposition of atomic charge densities, is well accounted for. Our results agree well with other ab initio calculations.^{34b,43-45} The smaller values of the (222) reflection obtained in Ref. 45 may be due to the limited number of Gaussian-type orbitals used in the wavefunction expansion.

B. CRYSTAL STABILITY

As described in Sec.^{III B}, total energies at several different lattice constants are calculated for seven crystal structures: the fcc, bcc, hcp, sc, CD, HD, and β -tin phases. These data are then least-squares fitted to the Murnaghan equation of state.²⁷ The fitted total energy curves as a function of atomic volume for the seven phases of Si and Ge are shown in Figs. 5 and 6. The minimum total energy per atom (E_{\min}), the relative total energy difference ΔE_{\min} ($\equiv E_{\min} - E_{\min}^{\text{CD}}$), and the corresponding atomic volume (V_{\min}) for each phase of Si and Ge

are given in Table V . We note that the value of E_{pw} controlling the plane wave expansion is 11.5 Ry. For this value, the difference ΔE_{min} between phases has already converged to 0.001 eV/atom while the absolute magnitude of E_{min} converges to only 0.02 eV/atom (Sec. VIA \wedge). Here we neglect the contribution from the zero-point vibration which has only small effects on the results to be reported.

The values for the β -tin phase given in Table VI and Figs. 5 and 6 are calculated using the experimental axial ratio⁵ (0.5516 for Si and 0.5512 for Ge). Total energy calculations have also been done for β -tin phases of different axial ratios (to be discussed in detail in the next subsection). From these calculations of the total energies of the seven phases, we find that the CD phase has the lowest E_{min} and is, thus, the most stable phase among the seven phases of Si and Ge. This is in agreement with experimental observation.

Compared to the CD phase, the HD phase has similar tetrahedral bonding character and differs only in the positions of the third nearest neighbors. It is expected that total energies for the two phases should be very close. Our calculations are not only consistent with this observation but they also show that the CD phase is more stable by a small energy difference (0.016 and 0.015 eV/atom for Si and Ge). The contour plot of valence charge density of the HD phase of Si at Ω_{expt} is shown in Fig. 7. The charge distribution is quite similar to that of the CD phase (Fig. 4).

For both Si and Ge, the other five phases are metallic

and have E_{\min} a few tenths an eV per atom higher than the CD phase. The ordering of phases as E_{\min} increases is β -tin, sc, bcc, hcp, and fcc. The V_{\min} 's (normalized to Ω_{expt}) of the metallic phases of Ge are larger than those of Si. This results from the filled 3d bands in Ge which exert a Pauli-type repulsion on the valence electrons having d-like character as manifested by the more repulsive d pseudopotential of Ge (Fig. 1). This effect is more appreciable in the metallic phases than in the sp^3 -bonded CD and HD phases.

Values of ΔE_{\min} of a few metallic phases of Si and Ge have been estimated from thermodynamical data. They are (in units of eV/atom) 0.46 and 0.53 for the bcc and hcp phases of Si^{46a} and 0.29 and 0.37 for the β -tin and fcc phases of Ge^{46b} respectively. These empirical values compare very well with our results (Table V). We note that the crystal stability of Si has been reported ^{in Ref. 35c} using a pseudopotential empirically fitted to excitation spectra. The diamond phase was found to be more stable than the β -tin, bcc, hcp, and fcc phases. However, the ΔE_{\min} 's between phases reported in Ref. 35c differ from the present results and the thermodynamically derived results.^{46a}

Since the structural properties of Si and Ge are qualitatively similar, we will concentrate on the results of Si in the following discussion. The contour plots of valence charge densities of the CD phase and the five metallic phases of Si at $0.751 \Omega_{\text{expt}}$ are shown in Fig. 8. (The contour plot for the HD phase is not shown because it is quite similar to that of the CD phase.) The maximum valence charge density between

nearest neighbors is a useful scale to gauge the covalent character: the CD and HD phases have large values of maximum valence charge density and, thus, strongly covalent character. Next come the β -tin and sc phases. The bcc, fcc, and hcp phases have the least covalent character. Notice the existence of prominent bond charge in the CD (as well as HD), β -tin, and sc phases.

The valence charge distribution around the atoms in the close-packed phases are reminiscent of the valence charge distribution in the atom. In fact, the charge density resulting from a superposition of atomic valence charge densities has similar peak positions and values. In Fig. 9, contour plots of the charge density so obtained⁴⁷ are shown in the (110) plane for the bcc phase of Si at $0.751 \Omega_{\text{expt}}$ and its difference from the corresponding self-consistent result (see Fig. 8). As the crystal forms, there is small charge pile-up between nearest neighbors. This effect becomes bigger as the covalent character increases. We note in passing that the charge distribution in the close-packed phases is quite spherically symmetric around the atoms, and this supports the use of spherical averaging procedures for close-packed crystals in some band structure methods such as the augmented-plane-wave method.⁴⁸

It is instructive to compare the contributions to the total energy [Eq. (1)] for different phases. The comparison of the individual energy contributions between the CD and the HD phases of Si and Ge at Ω_{expt} are shown in Table VI. The energy terms E'_{kin} , E'_H , and E'_{cc} favor the CD phase while E'_{xc} and E'_{ec} favor the HD phase. The signs of E'_H , E'_{cc} , and E'_{ec}

can be explained qualitatively by the observation that the distance to the third nearest neighbor is longer in the CD phase than in the HD phase. The values of E'_H and E'_{CC} are close, and they are almost cancelled by E'_{ec} . A slightly more localized charge distribution in the HD phase (see Figs. 4 and 7) seems to be the reason for the larger absolute magnitudes of E_{kin} and E_{xc} for the HD phase. (The computational error in the differences of the various energy contributions and the total energies is about 0.0003 Ry/atom.) Since the total energy differences are of the same order as or even smaller than the various energy terms, all energy terms are important in determining which of the CD and HD phases is more stable.

Incidentally, the structural relation between the cubic ZnS and hexagonal ZnS phases of ionic semiconductors is the same as that between the CD and HD phases of covalent semiconductors. The difference in Ewald energy (E'_{CC}) between the hexagonal form and the cubic form is reduced (in favor of the hexagonal form) by 0.0007 Ry/atom for the III-V compounds and 0.003 Ry/atom for the II-VI compounds with respect to the covalent counterpart at the measured Si volume. These values are comparable to the total energy difference between the CD and HD phases of Si and Ge. The favorable gain in the Ewald energy seems to be the reason why stable hexagonal ZnS structures are found in the II-IV compounds, for example, CdS, ZnS, and ZnSe.

The individual contributions to the total energy for the diamond, sc, β -tin, bcc, hcp, and fcc phases of Si (at $0.751 \Omega_{expt}^{Si}$) and Ge (at $0.742 \Omega_{expt}^{Ge}$) are given in Table VII. Note

that the change of the energy contributions between different phases correlates quite well with the nearest-neighbor distance, which in turn is closely related to the coordination number. The coordination numbers are 4, 6, 6, 8, 12, and 12, and the relative nearest-neighbor distances at the same atomic volume are 1, 1.155, 1.159, 1.260, 1.296, and 1.296 for the diamond, sc, β -tin, bcc, hcp, and fcc phases respectively. (The β -tin phase has four nearest neighbors and two second nearest neighbors at a 6% larger distance.) As the coordination number becomes smaller, the nearest-neighbor distance will usually become smaller if the atomic volume is kept the same. This causes a larger charge pile-up between nearest neighbors and a more localized valence charge distribution (Fig. 7). Thus, E_{kin} and E'_H will increase; E_{xc} and E'_{ec} will decrease; and the sum of these four terms [called the electronic contribution (E_e)] will decrease. The Ewald contribution (E'_{cc}), however, will usually increase because of the larger electrostatic potential energy between neighboring atomic cores. In other words, the electronic contribution favors phases of low coordination numbers while the Ewald contribution favors phases of high coordination numbers. Here the bcc, hcp, and fcc phases are regarded as one entity because their energy contributions are very close.

The total energies of the phases depend on the detailed balance between the electronic and the Ewald contributions. At the particular atomic volumes of Si and Ge (Table VII'), the relatively high Ewald contribution causes the total energy of the diamond phase to be larger than those of other phases.

Consequently, a phase transformation will occur before the diamond phase of Si or Ge, which is the most stable phase at zero pressure, is compressed to such small volumes. This topic will be discussed in the next subsection.

C. PRESSURE-INDUCED PHASE TRANSFORMATION

It is a well-known thermodynamic theorem that the phase transformation occurs when the Gibbs free energy

$$G \equiv E_{\text{tot}} + PV - TS, \quad (12)$$

becomes equal between the two phases. By applying this theorem to the zero-temperature case considered here, it is easily shown that the pressure-induced phase transformation occurs along the common tangent line between the $E_{\text{tot}}(V)$ curves of the two phases under consideration and the negative of the slope of the common tangent line is the transition pressure (P_t).

Although the HD phase of Si or Ge has the second lowest E_{min} , the common tangent between the HD and the CD energy curves either does not exist or has a slope much larger than that between the β -tin and the CD energy curves. Consequently, the HD phase is not the phase the CD phase will transform to under pressure. Since the HD energy curve lies slightly higher than the CD energy curve, the HD phase is a metastable phase having an equilibrium volume very close to that of the CD phase (Table V). The HD phase of Si has been experimentally observed¹⁰ to be metastable. Our calculated equilibrium volume for the HD phase is in excellent agreement with experiment.¹⁰

As can be seen from Figs. 5 and 6, the phase transformation to the β -tin phase has the smallest transition pressure among the possible pressure-induced phase transformations from the CD phase of Si or Ge. Thus our calculations show that under increasing hydrostatic pressure, the CD phase of Si or Ge will transform to the β -tin phase among the six possible choices for the transformed phase.

With increasing applied hydrostatic pressure, the crystals of Si and Ge will follow the path 1 \rightarrow 2 \rightarrow 3 \rightarrow 4 as shown in Figs. 5 and 6. The phase transformation occurs along the path 2 \rightarrow 3. This segment represents a mixture of these two phases. The initial and final transition volumes (V_t^d and V_t^β) are determined from the tangent points. The calculated transition volumes and transition pressures of Si and Ge are given in Table IX along with the experimental values.^{5,7-9} The agreement for the transition volumes are excellent. The differences between theory and experiment are only a few percent. The transition pressures have a larger discrepancy. While the calculated transition pressures are for zero-temperature, the experimental transition pressures were measured at room temperature.⁷⁻⁹ Using the phase diagrams shown in Ref. 49, we estimate that the transition pressure may change by $\lesssim \pm 15\%$ from room temperature to 0 K. In addition, possible superstress effects may cause the measured value to be higher than the theoretical value and the theoretical value itself has a large uncertainty (Appendix C). Thus, the agreement of the calculated transition pressures with experiment is considered to be quite

satisfactory.

There is an interesting structural relationship between the CD phase and the β -tin phase. Shown in Fig. 10 is a ball and stick model of the diamond crystal structure in dashed cubic cells. A tetragonal unit cell can equally well be chosen to represent the crystal structure as indicated by solid lines in Fig. 10. The space lattice of the diamond crystal structure is then body-centered tetragonal with an axial ratio (c/a) of 2. The observed β -tin phases belong to the same lattice class but with a much smaller axial ratio [0.552 for Si (Ref. 5), 0.551 for Ge (Ref. 5), and 0.546 for the real β -tin (Ref. 31)].

Calculations have been carried out for several β -tin structures of Si and Ge with axial ratios varied within 20% of the observed values. The calculated total energy curves of Si for the diamond phase and the β -tin phases with axial ratios 0.458, 0.488, 0.552, and 0.621 are shown in Fig. 11. The energy curve with axial ratio 0.46 lies above the other curves. As the axial ratio increases, the energy curve moves downward. After the axial ratio reaches the value 0.55, the energy curves moves upward again. It is clear from Fig. 11 that the transformed β -tin phase under hydrostatic pressure has axial ratio close to 0.55. When we vary the axial ratio within 5% of the value 0.55, the calculated total energy curves differ from each other by less than 0.4 mRy/atom and are essentially indistinguishable from the curve (i) if drawn in Fig. 11. Consequently, the theoretical estimate of the axial ratio of the pressure-transformed β -tin phase of Si is $0.55 \pm 5\%$. A similar treatment has also

been done for Ge. The calculated axial ratio is also $0.55 \pm 5\%$. These values agree quite well with the experimental values⁵ of 0.552 (Si) and 0.551 (Ge).

It is instructive to analyze the individual energy contributions to the total energy as the axial ratio of the β -tin phase varies. Figure 12 shows the individual energy contributions and total energy of the β -tin phase of Si as a function of the axial ratio at a fixed atomic volume ($0.71 \Omega_{\text{expt}}$). The minimum of the Ewald energy (E'_{CC}) has an axial ratio of 0.5445 at which the second-nearest-neighbor distance is very close to the nearest-neighbor distance and the effective coordination number is six instead of two or four. It is a rule of thumb that the Ewald energy favors high coordination numbers and evenly distributed atoms in the crystal. The total energy also has a minimum close to the axial ratio 0.55 and it is a shallow minimum. We may argue that the Ewald energy E'_{CC} plays a dominant role in determining the equilibrium axial ratio. The electronic contribution E_e serves as electronic screening and reduces the effect of the Ewald contribution. This is supported by the fact that the observed axial ratios are very close to the minimum axial ratio of the Ewald energy. We note that the minima of E_{kin} and E'_H and the maxima of E'_{ec} and E_{xc} are also in the vicinity of axial ratio 0.55, which are related to the fact that the valence electrons are more uniformly distributed around that axial ratio.

In contrast, the Ewald contribution does not favor the diamond phase. Figure 13 plots the Ewald constant, which is

proportional to the Ewald energy for a fixed volume, as a function of the axial ratio. While the observed β -tin phase is in the vicinity of a local minimum, the diamond phase corresponds to a local maximum.⁵⁰ This unfavorable Ewald contribution is more than compensated by the electronic contribution (E_e) for the diamond phase at Ω_{expt} as indicated in Fig. 14 in which we plot the differences between various contributions to the total energy of the diamond and the β -tin phase ($c/a = 0.552$) of Si as a function of atomic volume. Figure 14 also shows that E_{ec} and E_{xc} favor the diamond phase and E_{kin} and E_{H} favor the β -tin phase. When the atomic volume decreases under pressure, the system becomes more metallic and the stabilizing effect of the electronic contribution (ΔE_e) for the diamond phase becomes weaker with respect to the opposing Ewald contribution ($\Delta E'_{\text{cc}}$). At the transition pressure, the gain in Ewald energy becomes so favorable relative to the β -tin phase that the phase transformation occurs, i.e., the Ewald contribution is the driving mechanism for this diamond- β -tin phase transformation.

D. ELECTRONIC STRUCTURES

In this subsection, we present the results of electronic structure calculations for the diamond phase of Si and Ge at Ω_{expt} .³¹ The electronic structures of Si and Ge shown in Figs. 15 and 16 are calculated using a plane wave basis set with a kinetic energy cutoff (E_{pw}) of 11.5 Ry at which point the overall convergent error of eigenvalues is about 0.05 eV. The s-like antibonding conduction state Γ_2 , has a large convergent error. It changes from 3.39 eV to 3.29 eV for Si and from

1.01 eV to 0.73 eV for Ge when E_{pw} is increased from 11.5 Ry to 20 Ry. For $E_{pw} = 20$ Ry, the overall convergent error of eigenvalues is 0.01 eV. (The Schrödinger equation is solved self-consistently for each E_{pw} .)

In Table IX we listed the eigenvalues at Γ , X, and L of Si and Ge calculated using $E_{pw} = 11.5$ Ry and 20 Ry. These values agree quite well with other ab initio calculations.^{34c,45,51-53} In particular, the differences in eigenvalue between our results and the all-electron LAPW calculation⁵² of Si are only about 0.1 eV.

Since the density-functional formalism was developed only for ground-state properties, the calculated eigenvalues do not correspond directly to elementary excitations. Nevertheless, a comparison of the calculated values with experimental excitation spectra may provide some clue to the construction of a fundamental theory for elementary excitations. The density of states for Si and Ge are displayed in Figs. 17 and 18. The peak positions agree quite well with the angle-integrated photoemission spectra.⁵⁴⁻⁵⁶ In Table X, we compare our results with experiments at critical points. It seems that the calculated results can explain the peak positions in the photoemission spectra rather well with an overall error of about 0.3 eV.

On the other hand, the comparison with the optical measurements shows large errors. The calculated indirect gaps are 0.48 eV from Γ to 0.85X for Si and 0.47 eV from Γ to L for Ge. The experimental values are 1.17 eV⁵⁷ from Γ to 0.82X⁵⁸ for Si and 0.74 eV from Γ to L⁵⁹ for Ge. While the calculated positions

in the Brillouin zone for the valence band maximum and the conduction band minimum are in good agreement with experiment, the magnitudes of the energy gaps are underestimated. This seems to be a general phenomenon in the ab initio density-functional calculations. The calculated direct gaps are 2.54 eV ($\Gamma_{25'} \rightarrow \Gamma_{15}$) for Si and 0.73 eV ($\Gamma_{25'} \rightarrow \Gamma_{2'}$) for Ge. Again, these values are lower than the experimental values of 2.74 eV for Si⁶⁰ and 0.89 eV for Ge,⁶¹ but by a smaller amount (0.2 eV).

IV. CONCLUSIONS

In summary we present an extensive microscopic study of the structural properties of two group-IV elemental crystals: Si and Ge, employing an ab initio pseudopotential method¹⁸ within the local-density-functional formalism.² Using atomic numbers of the constituent elements and a subset of crystal structures (diamond, hexagonal diamond, β -tin, sc, bcc, hcp, and fcc) as the only input information, the calculated structural properties are in excellent agreement with experiment. They included: (i) the static structural properties such as lattice constants, cohesive energies, and bulk moduli; (ii) the crystal stability such as the determination of the most stable phase; and (iii) properties of pressure-induced phase transformation.

In particular, our calculations show that the diamond phase of Si and Ge is the most stable phase among the seven phases under consideration and it will transform to the β -tin phase under hydrostatic pressure. The transition volumes, transition pressures, along with the axial ratio of the final β -tin phase in the pressure-induced phase transformation agree

very well with experiment. We also show that the Ewald energy is the driving force for this pressure-induced diamond- β -tin phase transformation. The present results along with the results¹ of lattice dynamical properties demonstrate that not only the static structural properties of crystals but also the other important structural properties of the crystal stability, phase transformation, and lattice dynamics can be accurately described from first principles within the local-density-functional formalism.

ACKNOWLEDGMENT

This work was supported by National Science Foundation Grant No. DMR7822465 and by the Director, Office of Energy Research, Office of Basic Energy Sciences, Materials Sciences Division of the U.S. Department of Energy under Contract No. DE-AC03-76SF00098.

APPENDIX A

In this appendix, we give the results of the convergence test of the static properties with respect to the kinetic energy cutoff (E_{pw}) for the plane wave basis set (Table XI). The lattice constant converges quite fast, e.g., it has already converged to within 1% at $E_{pw} = 4.3$ Ry for Si. At $E_{pw} = 11.5$ Ry, the lattice constants converge to better than 1%, and the cohesive energies and the bulk moduli converge to about 5%.

APPENDIX B

In this appendix, we discuss the accuracy of the pseudopotential approximation in which an ab initio pseudopotential is used to simulate the interaction between the valence electrons and the atomic core. Shown in Fig. 19 is another ab initio pseudopotential of Si generated²² using a reference configuration of $3s^2 3p^{0.5} 3d^{0.5}$, and r_c values (in a.u.) of 1.35, 1.56, 1.56 for the s, p, and d component of the pseudopotential. While the pseudopotentials shown in Fig. 1(a) and Fig. 19 are quite different, the calculated equilibrium lattice constant, the cohesive energy, and the bulk modulus differ by only 0.5%, 1%, and 2% respectively. We have also tested other generation schemes⁶² for ab initio pseudopotentials and obtained similar results. This demonstrates that the structural properties do not depend appreciably on the pseudopotential generating scheme and the parameters used in the scheme as long as the generated pseudopotential is capable of reproducing all-electron atomic results for a wide range of atomic configurations (see Sec. III). We also note that the pseudopotential approximation works best for cases in which the valence wavefunctions do not overlap appreciably with the core wavefunctions as in the present case. When the overlaps are not negligible (as in the case of Na), significant error will result⁶³ from the fact that $V_{xc}(\rho)$ [Eq. (10)] is a nonlinear function of the charge density. It has been shown⁶³ that such errors can be eliminated by including core charge effects in the treatment of the exchange-correlation potential and energy.

APPENDIX C

In this appendix, we examine the variation of the calculated structural properties with respect to the functional form of $E_{xc}[\rho]$. If the exchange-correlation form (E_{xc}^{HL}) proposed by Hedin and Lundqvist (HL)⁶⁴ is used in the calculation of the static properties of Si, the resulting lattice constant decreases by 1%, and the cohesive energy and the bulk modulus increase by 5% as compared to the corresponding results using the Wigner form E_{xc}^W .

The variations in the lattice constant and the cohesive energy can be qualitatively explained directly from the different functional forms of $E_{xc}[\rho]$. In the zeroth-order approximation, the exchange-correlation contribution to the total energy per atom is $Z_V \epsilon_{xc}(\bar{\rho})$ where Z_V is the number of valence electrons and $\bar{\rho}$ the average valence charge density. Compared with the Wigner form of ϵ_{xc} , the HL form decreases faster as $\bar{\rho}$ increases, viz. it favors high charge density and small lattice constant. This also leads to a larger cohesive energy calculated using the HL form because the overall valence charge density of the crystal is larger than that of isolated atoms.

As for the study of crystal stability, ΔE_{min} between the CD and the HD phases varies by less than 10^{-3} eV/atom when different E_{xc} 's are used. This is because both phases have almost the same equilibrium atomic volume and similar valence charge distributions. The difference ΔE_{min} between the other five phases and the CD phase is lowered by about 0.02 eV/atom when E_{xc}^{HL} is used instead of E_{xc}^W . This results from the fact

that these five phases have smaller equilibrium atomic volume and that E_{xc}^{HL} favors small atomic volume. Such variations in ΔE_{min} do not effect our conclusions about the crystal stability.

Since E_{xc}^{HL} favors small atomic volume, the calculated transition pressure for the diamond- β -tin phase transformation using E_{xc}^{HL} is 10% smaller than that using E_{xc}^W . The transition volumes have only small variations, they decrease by 1% when E_{xc}^{HL} is used instead of E_{xc}^W .

Other functional forms³⁰ of $E_{xc}[\rho]$ have also been examined, the results are similar to those discussed above. It should be noted that the expression of $E_{xc}[\rho]$ in Eq. (2) is itself an approximation (the local-density-functional approximation²).

References

- [†]Present address: Bell Laboratories, Murray Hill, NJ 07974
- ¹M. T. Yin and M. L. Cohen, (a) Phys. Rev. Lett. 45, 1004 (1980); and Solid State Commun. 38, 625 (1981).
- ²P. Hohenberg and W. Kohn, Phys. Rev. 136, B864 (1964); W. Kohn and L. J. Sham, Phys. Rev. 140, A1133 (1965).
- ³See, e.g., V. L. Moruzzi, J. F. Janak, and A. R. Williams, Calculated Electronic Properties of Metals (Pergamon, New York, 1978).
- ⁴S. Minomura and H. G. Drickamer, J. Phys. Chem. Solids 23, 451 (1962). The transition pressures reported are corrected by the revised calibration for high pressure (H. G. Drickamer, Rev. Sci. Instrum. 41, 1667 (1970)).
- ⁵J. C. Jamieson, Science 139, 762 and 845 (1963).
- ⁶See M. C. Gupta and A. L. Ruoff, J. Appl. Phys. 51, 1072 (1980) for a rather complete table of results of high-pressure studies on Si.
- ⁷G. J. Piermarini and S. Block, Rev. Sci. Instrum. 46, 973 (1975).
- ⁸B. A. Weinstein and G. J. Piermarini, Phys. Rev. B 12, 1172 (1975).
- ⁹K. Asaumi and S. Minomura, J. Phys. Soc. Japan 45, 1061 (1978).
- ¹⁰R. H. Wentorf and J. S. Kasper, Science 139, 338 (1962).
- ¹¹C. H. Bates, F. Dacheille, and R. Roy, Science 147, 860 (1965).
- ¹²F. P. Bundy and J. S. Kasper, Science 139, 340 (1963); J. S. Kasper and S. M. Richards, Acta Cryst. 17, 752 (1964).
- ¹³J. C. Phillips, Phys. Rev. Lett. 27, 1197 (1971); Bonds and Bands in Semiconductors (Academic Press, New York, 1973).

- ¹⁴ J. A. Van Vechten, Phys. Status Solidi (b) 47, 261 (1971) and Phys. Rev. B 7, 1479 (1972).
- ¹⁵ D. Penn, Phys. Rev. 128, 2093 (1962).
- ¹⁶ A. Morita and T. Soma, Solid State Commun. 11, 927 (1972);
T. Soma, J. Phys. C 11, 2681 (1978).
- ¹⁷ W. Andreoni and K. Maschke, Phys. Rev. B 22, 4816 (1980).
- ¹⁸ See, e.g., M. T. Yin and M. L. Cohen, to be published.
- ¹⁹ A. K. McMahan, M. T. Yin, and M. L. Cohen, Phys. Rev. B

- ²⁰ J. Ihm, A. Zunger, and M. L. Cohen, J. Phys. C 12, 4409 (1979);
M. T. Yin and M. L. Cohen, to be published.
- ²¹ See J. Ihm and M. L. Cohen, Phys. Rev. B 21, 3754 (1980) and references therein.
- ²² D. R. Hamann, M. Schlüter, and C. Chiang, Phys. Rev. Lett. 43, 1494 (1979).
- ²³ E. Wigner, Phys. Rev. 46, 1002 (1934).
- ²⁴ M. Schlüter, J. R. Chelikowsky, S. G. Louie, and M. L. Cohen, Phys. Rev. B 12, 4200 (1975).
- ²⁵ D. J. Chadi and M. L. Cohen, Phys. Rev. B 8, 5747 (1973);
H. J. Monkhorst and J. D. Pack, Phys. Rev. B 13, 5189 (1976).
- ²⁶ O. Jepsen and O. K. Anderson, Solid State Commun. 9, 1763 (1971); G. Lehmann and M. Taut, Phys. Status Solidi B 54, 469 (1972).
- ²⁷ For the total energy calculation of the bcc and fcc phases of Si reported in Ref. 1(a), the tetrahedron method was used. The convergent error was about 0.05 Ry/atom using 20 k points (for fcc) and 30 k points (for bcc) in the irreducible Brillouin

zone. The present calculation for these two phases has a better convergency (0.001 Ry/atom).

²⁸ (a) F. D. Murnaghan, Proc. Nat. Acad. Sci. U.S.A. 30, 244 (1944); (b) O. L. Anderson, J. Phys. Chem. Solids 27, 547 (1966).

²⁹ We neglect the effect of lattice vibrations which is estimated to cause about 0.1% and 1% errors in the equilibrium lattice constant and the bulk modulus respectively.

³⁰ U. von Barth and L. Hedin, J. Phys. C 5, 1629 (1972); O. Gunnarsson, B. I. Lundqvist, and J. W. Wilkins, Phys. Rev. B 10, 1319 (1974).

³¹ The experimental zero-pressure lattice constants and atomic volumes (Ω_{expt}) at 0 K are obtained from J. Donohue, The Structures of Elements (Wiley, New York, 1974), corrected for thermal expansion and atmospheric-pressure compression.

³² L. Brewer, Lawrence Berkeley Laboratory Report No. LB-3720 (unpublished), May 1977 revision (for the cohesive energy at 0 K); C. E. Moore, Atomic Energy Levels (National Bureau of Standards, Washington D.C., 1949), Circular No. 467, Vol. I.

³³ H. J. McSkimin, J. Appl. Phys. 24, 988 (1953); H. J. McSkimin and P. Andreatch, Jr., ibid. 34, 651 (1963) and 35, 2161 (1964). The elastic moduli were measured at 77 K.

³⁴ (a) J. A. Vergés and C. Tejedor, Phys. Rev. B 20, 4251 (1979); (b) A. Zunger, Phys. Rev. B 21, 4785 (1980); (c) D. Glotzel, E. Segall, and O. K. Anderson, Solid State Commun. 36, 403 (1980).

³⁵ (a) A. Morita, T. Soma, and J. Takeda, J. Phys. Soc. Jpn.

- 32, 29 (1972); (b) H. Wendel and R. M. Martin, Phys. Rev. Lett. 40, 950 (1978), and Phys. Rev. ^B19, 5251 (1979); (c) J. Ihm and M. L. Cohen, Solid State Commun. 29, 711 (1979), and Phys. Rev. B 21, 1527 (1980).
- ³⁶J. F. Janak, V. L. Moruzzi, and A. R. Williams, Phys. Rev. B 12, 1257 (1975).
- ³⁷G. Dolling, Inelastic Scattering of Neutrons in Solids and Liquids (IAEA, Vienna, 1963), Vol. II, p. 37; G. Nilson and G. Nelin, Phys. Rev. B 3, 364 (1971).
- ³⁸We have examined the convergency of the valence charge density with respect to E_{pw} (the kinetic energy cutoff in the plane-wave expansion). The peak values (in units of electrons per atomic volume) changed from 11.7 to 11.5 for Si and from 11.35 to 11.3 for Ge when E_{pw} is increased from 11.5 Ry to 20 Ry. The peak positions move away from the bond center in the bonding direction by about 4% of the bond length for Si (5% for Ge). The changes in the valence contributions to the x-ray structural factors are about 0.01 e/cell.
- ³⁹Y. W. Yang and P. Coppins, Solid State Commun. 15, 1555 (1974).
- ⁴⁰P. J. E. Aldred and M. Hart, Proc. R. Soc. London A332, 223 (1973).
- ⁴¹J. B. Roberto, B. W. Batterman, and D. T. Keating, Phys. Rev. B 15, 2590 (1974) [for (222) reflection of Si].
- ⁴²T. Matsushita and K. Kohra, Phys. Status Solidi A24, 531 (1974).
- ⁴³P. M. Raccach, R. N. Euwema, D. J. Stukel, and T. C. Collins, Phys. Rev. B 1, 756 (1970).

- ⁴⁴R. Heaton and E. Lafon, J. Phys. C 14, 347 (1981).
- ⁴⁵C. S. Wang and B. M. Klein, Phys. Rev. B 24, 3393 (1981).
- ⁴⁶(a) L. Kaufman and H. Nesor, in Titanium Science and Technology, edited by R. I. Jaffe and H. Burte (Plenum, New York, 1973), Vol. 2, p. 773; (b) A. P. Miodownik, in Metallurgical Chemistry, Proceedings of Metallurgical Chemistry Symposium, Brunel University and National Physical Laboratory, London, ed. O. Kubaschewski (H.M.S.O., London, 1972). We thank Dr. D. G. Pettifor and Dr. L. Kaufman for bringing these empirical results to our attention.
- ⁴⁷The pseudo valence charge density of the atom with configuration $3s^1 3p^3$ is used.
- ⁴⁸See, e.g., T. L. Loucks, Augmented Plane Wave Method (Benjamin, New York, 1967).
- ⁴⁹A. Jayaraman, W. Klement, Jr., and G. C. Kennedy, Phys. Rev. 130, 540 (1963); F. P. Bundy, J. Chem. Phys. 41, 3809 (1964).
- ⁵⁰D. Weaire, Phys. Status Solidi 42, 767 (1970).
- ⁵¹D. J. Stukel and R. N. Euwema, Phys. Rev. B 1, 1635 (1970).
- ⁵²D. R. Hamann, Phys. Rev. Lett. 42, 662 (1979).
- ⁵³A. Zunger and M. L. Cohen, Phys. Rev. B 20, 4082 (1979).
- ⁵⁴L. Ley, S. Kowalczyk, R. Pollak, and D. A. Shirley, Phys. Rev. Lett. 29, 1088 (1972). Their experimental values are quoted in J. R. Chelikowsky and M. L. Cohen, Phys. Rev. B 10, 5095 (1974).
- ⁵⁵W. D. Grobman and D. E. Eastman, Phys. Rev. Lett. 29, 1508 (1972); W. D. Grobman, D. E. Eastman, and J. L. Freeouf, Phys. Rev. B 12, 405 (1975).

- ⁵⁶W. E. Spicer and R. Eden, in Proceedings of the Ninth International Conference of the Physics of Semiconductors, 1968 (Nauka, Leningrad, 1968), Vol. 1, p. 61.
- ⁵⁷K. L. Shalee and R. E. Nahony, Phys. Rev. Lett. 24, 942 (1970).
The indirect band gap of Si was measured at 1.8 K.
- ⁵⁸See W. P. Dunke, Phys. Rev. 118, 938 (1960) and references therein.
- ⁵⁹C. Kittel, Introduction to Solid State Physics, 5th ed. (Wiley, New York, 1975), p. 210.
- ⁶⁰G. K. M. Thutupalli and S. G. Tomlin, J. Phys. C 10, 467 (1977).
- ⁶¹H. Piller and V. A. Patton, Phys. Rev. 129, 1169 (1963).
The direct gap of Ge was measured at 77 K.
- ⁶²G. Kerker, J. Phys. C 13, L189 (1980).
- ⁶³S. G. Louie, S. Froyen and M. L. Cohen (to be published).
- ⁶⁴L. Hedin and B. I. Lundqvist, J. Phys. C 4, 2064 (1971).

TABLE I. Eigenvalues and excitation energies of the pseudoatom for different atomic configurations of Si and Ge. Energies are in Rydbergs. The method in Ref. 22 is employed to generate the pseudopotentials using $s^2p^{0.5}d^{0.5}$ reference configuration and Wigner correlation.²³ The values in parentheses are deviations from the corresponding all-electron results.

Configuration	Eigenvalues			Excitation energy (ΔE_{tot})
	s	p	d	
<u>Si</u>				
$3s^2 3p^2$	-0.7994 (-0.0014)	-0.3126 (-0.0006)		0
$3s^1 3p^3$	-0.8538 (-0.0008)	-0.3543 (-0.0004)		0.4932 (0.0006)
$3s^1 3p^{2.5} 3d^{0.5}$	-1.0226 (-0.0008)	-0.5048 (-0.0006)	-0.0380 (0.0001)	0.7030 (0.0009)
$3s^2 3p^{0.5} 3d^{0.5}$	-1.4851 (0.0000)	-0.9420 (0.0000)	-0.3364 (0.0000)	(0.0009) (0.0000)
$3s^2 3p^0$	-2.0948 (0.0028)	-1.5154 (0.0024)		1.7640 (0.0005)

Continued on the following page.

Ge

$4s^2 4p^2$	0.8350 (-0.0015)	0.3061 (-0.0008)		0
$4s^1 4p^3$	0.9202 (0.0001)	0.3533 (-0.0006)		0.5582 (0.0000)
$4s^1 4p^2 4d^1$	1.2155 (0.0017)	0.6075 (0.0003)	0.0607 (0.0000)	1.0238 (0.0004)
$4s^2 4p^0$	2.1342 (0.0030)	1.4745 (0.0026)		1.7218 (0.0002)

TABLE II. Comparison of calculated and measured static properties of Si and Ge.

	Lattice constant (Å)	Cohesive energy (eV/atom)	Bulk modulus (Mbar)
<u>Si</u>			
calculation	5.451	4.84 ^b	0.98 ^c
experiment	5.429 ^a	4.63 ^b	0.99 ^c
<u>Ge</u>			
calculation	5.655	4.26 ^b	0.73 ^c
experiment	5.652 ^a	3.85 ^b	0.77 ^c

^aRef. 31 (0 K)

^bRef. 32 (0 K)

^cRef. 33 (77 K)

TABLE III. Comparison of various energy contributions (in units of Ry/atom) to the total energy between the (pseudo) atom and the crystal for Si and Ge.

	atom	crystal	diff.
<u>Si</u>			
E_{kin}	2.518	3.015	0.497
E_{xc}	-1.926	-2.381	-0.455
E_{pot}	-9.095	-8.555	-0.460
E_{spin}	-0.058	0	0.058
E_{vib}	0	0.005	0.005
E_{tot}	-7.561	-7.916	-0.355
<u>Ge</u>			
E_{kin}	2.511	2.844	0.333
E_{xc}	-1.910	-2.312	-0.402
E_{pot}	-8.135	-8.438	-0.303
E_{spin}	-0.056	0	0.056
E_{vib}	0	0.003	0.003
E_{tot}	-7.590	-7.903	-0.313

TABLE IV. Comparison of calculated x-ray structure factors for Si and Ge with experiment (in units of electron per primitive cell).

	Si		Ge	
	Theory	Expt. ^a	Theory	Expt. ^b
000	28.00	(28.00)	64.00	(64.00)
111	15.13	15.19	38.85	39.42
220	17.23	17.30	47.26	47.44
311	11.28	11.35	31.24	31.37
222	0.34	0.38	0.28	0.27
400	14.76	14.89	40.47	40.50
331	10.11	10.25	27.37	27.72
422	13.22	13.42	35.84	36.10
333	8.92	9.09	24.26	24.50
511	8.96	9.11	24.28	
440	11.88	12.08	32.14	32.34

^aRefs. 40 and 41

^bRef. 42

TABLE V . The volumes at the minimum structural energies (V_{\min} , normalized to measured free volume), the minimum energies (E_{\min}), and ΔE_{\min} ($\equiv E_{\min} - E_{\min}^{\text{diamond}}$) for the seven plausible structures of Si and Ge.

	Diamond	Hexagonal Diamond	β -tin	sc	bcc	hcp	fcc
<u>Si</u>							
V_{\min}	1.012	1.015	0.773	0.808	0.736	0.723	0.733
E_{\min} (Ry)	-7.9086	-7.9074	-7.889	-7.883	-7.870	-7.868	-7.867
ΔE_{\min} (eV)	0	0.016	0.27	0.35	0.53	0.55	0.57
<u>Ge</u>							
V_{\min}	1.003	1.003	0.802	0.839	0.795	0.805	0.816
E_{\min} (Ry)	-7.8885	-7.8874	-7.870	-7.866	-7.856	-7.855	-7.854
ΔE_{\min} (eV)	0	0.015	0.25	0.31	0.44	0.45	0.46

TABLE VI . Comparison between various contributions to the total energy of the cubic diamond (CD) and the hexagonal diamond (HD) phase at Ω_{expt} (Ref. 31). The energies are in units of Ry/atom. E_e is the electronic contribution which is the sum of E_{kin} , E_{xc} , E'_H , and E'_{ec} .

	<u>Si</u>			<u>Ge</u>		
	CD	HD	CD-HD	CD	HD	CD-HD
E_{kin}	3.0001	3.0007	-0.0006	2.8295	2.8311	-0.0016
E_{xc}	-2.3782	-2.3784	0.0002	-2.3096	-2.3100	0.0004
E'_H	0.5322	0.5435	-0.0113	0.5471	0.5587	-0.0116
E'_{ec}	-0.6632	-0.6861	0.0229	-0.8920	-0.9156	0.0236
E_e	0.4909	0.4797	-0.0112	0.1750	0.1642	-0.0108
E'_{cc}	-8.3995	-8.3871	-0.0124	-8.0634	-8.0516	-0.0118
E_{tot}	-7.9086	-7.9074	-0.0012	-7.8884	-7.8874	-0.0010

TABLE VII . Comparison of various contributions to the total energy (Eq. 1) for the diamond, sc, β -tin, bcc, hcp, and fcc phases of Si (at $0.751 \Omega_{\text{expt}}^{\text{Si}}$) and Ge (at $0.742 \Omega_{\text{expt}}^{\text{Ge}}$). The energies are in units of Ry/atom. E_e is the electronic contribution, which is the sum of E_{kin} , E_{xc} , E'_H , and E'_{ec} .

	diamond	sc	β -tin	bcc	hcp	fcc
<u>Si</u> ($0.751 \Omega_{\text{expt}}$)						
E_{kin}	3.4195	3.1081	3.0674	2.9896	2.9855	2.9855
E_{xc}	-2.5366	-2.4379	-2.4283	-2.4037	-2.4033	-2.4035
E'_H	.4200	.1121	.0842	.0332	.0351	.0356
E'_{ec}	0.073	1.0698	1.1928	1.4199	1.4229	1.4235
E_e	1.3764	1.8520	1.9162	2.0390	2.0397	2.0412
E'_{cc}	-9.2394	-9.7330	-9.8046	-9.9085	-9.9075	-9.9079
E_{tot}	-7.8630	-7.8809	-7.8884	-7.8695	-7.8678	-7.8667

Continued on the following page.

Ge (0.742 Ω_{expt})

E_{kin}	3.2103	2.9414	2.9035	2.8468	2.8470	2.8456
E_{xc}	-2.4651	-2.3713	-2.3507	-2.3378	-2.3380	-2.3377
E'_{H}	.4237	.1266	.0955	.0451	.0477	.0477
E'_{ec}	-0.1138	.8225	.9421	1.1395	1.1373	1.1401
E_{e}	1.0551	1.5191	1.5803	1.6935	1.6940	1.6957
E'_{cc}	-8.9034	-9.3791	-9.4481	-9.5482	-9.5472	-9.5476
E_{tot}	-7.8483	-7.8600	-7.8678	-7.8546	-7.8532	-7.8518

TABLE VIII. Comparison of the calculated and measured transition volumes ($V_t^{d,\beta}$) of the diamond and β -phases, their ratios (V_t^β/V_t^d), and the transition pressures (P_t) for Si and Ge. The volumes are normalized to the measured zero-pressure volumes.³¹

	V_t^d	V_t^β	V_t^β/V_t^d	P_t (kbar)
<u>Si</u>				
calculation	0.928	0.718	0.774	99
experiment	0.918 ^a	0.710 ^a	0.773 ^a	125 ^b
deviation	1.1%	1.1%	0.1%	-20%
<u>Ge</u>				
calculation	0.895	0.728	0.813	96
experiment	0.875 ^a	0.694 ^a	0.793 ^a	100 ^c
deviation	2.3%	4.9%	2.5%	-4%

^aRef. 5

^bRefs. 78

^cRef. 9

TABLE IX. Eigenvalues of Si and Ge in eV at Γ , X, and L calculated using $E_{pw} = 11.5$ Ry and 20 Ry which correspond to about 180 and 400 plane waves respectively. The energies in eV are measured from the valence band maximum ($\Gamma_{25'}$).

E_{pw}	Si		Ge	
	11.5 Ry	20 Ry	11.5 Ry	20 Ry
Γ_1	11.95	-11.93	-12.48	-12.48
$\Gamma_{25'}$	0	0	0	0
Γ_{15}^C	2.54	2.53	2.53	2.55
$\Gamma_{2'}^C$	3.39	3.29	1.01	0.73
Γ_1^C	7.66	7.63	6.45	6.41
X_1	-7.80	-7.78	-8.58	-8.57
X_4	-2.92	-2.88	-3.08	-3.04
X_1^C	0.62	0.61	0.71	0.73
X_3^C	9.99	9.97	9.53	9.54
$L_{2'}$	-9.57	-9.52	-10.39	-10.36
L_1	-7.01	-7.00	-7.42	-7.41
$L_{3'}$	-1.23	-1.20	-1.41	-1.39
L_1^C	1.52	1.48	0.51	0.47
L_3^C	3.37	3.31	3.67	3.70
$L_{2'}^C$	7.48	7.48	6.96	6.99

TABLE X . Comparison of the peak positions in the calculated valence-band density of states with those in angle-integrated photoemission spectra. Energies in eV are measured from the valence band maximum.

	<u>Si</u>		<u>Ge</u>	
	Theory	Experiment	Theory	Experiment
Γ_1	-11.93	-12.4 \pm 0.6 ^a -12.5 \pm 0.6 ^b	-12.48	-12.6 \pm 0.3 ^a -12.8 \pm 0.4 ^b
$L_{2'}$	-9.52	-9.3 \pm 0.4 ^b	-10.36	-10.6 \pm 0.95 ^a -10.5 \pm 0.4 ^b
L_1	-7.00	-6.4 \pm 0.4 ^a -6.8 \pm 0.2 ^b	-7.41	-7.7 \pm 0.2 ^a -7.4 \pm 0.2 ^b
Σ_1	-4.52	-4.7 \pm 0.2 ^{a,b} -4.4 ^c	-4.51	-4.5 \pm 0.2 ^{a,b}
X_4	-2.88	-2.5 \pm 0.3 ^b	-3.04	3.2 \pm 0.2 ^a
$L_{3'}$	-1.20	-1.2 \pm 0.2 ^c	-1.39	-1.1 \pm 0.2 ^a -1.4 \pm 0.2 ^c

^aRef. 55

^bRef. 54

^cRef. 56

TABLE XI . Convergent test of the static properties of Si and Ge with respect to the kinetic energy cutoff (E_{pw}) of the plane wave basis set.

E_{pw} (Ry)	lattice constant (Å)	cohesive energy (eV/atom)	bulk modulus (Mbar)
<u>Si</u>			
3.5	5.467	1.84	1.76
4.3	5.386	2.56	1.29
6.0	5.394	3.45	0.97
8.0	5.439	4.11	1.01
11.5	5.451	4.67	0.98
Expt. ^a	5.429	4.63	0.99
<u>Ge</u>			
6.0	5.551	2.41	0.89
8.0	5.599	3.24	0.79
11.5	5.655	4.02	0.73
Expt. ^a	5.652	3.85	0.77

^aRefs. 31, 32, and 33

Figure Captions

Fig. 1 Ab initio core pseudopotentials of (a) Si and (b) Ge generated²² using the reference valence configuration of $s^2 p^{0.5} d^{0.5}$. The letters s, p, and d denote the nonlocal pseudopotential for angular momenta $l = 0, 1, \text{ and } 2$ respectively. The dashed line denotes the Coulomb potential of a (fictitious) point-like atomic core.

Fig. 2 The comparison between the pseudo (solid lines) and the corresponding all-electron (dashed lines) radial wavefunctions for the configurations $3s^2 3p^2$ and $3s^1 3p^2 3d^1$ of Si.

Fig. 3 Convergence test of the calculated cohesive energy (E_{coh}) of Si with respect to the kinetic energy cutoff (E_{pw}) of the plane wave basis set (N_{pw} is the approximate number of the plane waves in the basis set).

Fig. 4 Contour plots of the valence charge density in the (110) plane of the cubic diamond (CD) phase of Si and Ge at Ω_{expt} (Ref. 31). The charge density is in units of electrons per atomic volume with a contour step of 1. The black dots denote the atomic positions and straight lines denote the atomic chains.

Fig. 5 Total energy curves of the seven phases of Si as a function of the atomic volume normalized to Ω_{expt} (Ref. 31). The dashed line is the common tangent of the energy curves for the diamond phase and the

β -tin phase ($c/a = 0.552$).

- Fig. 6 Total energy curves of the seven phases of Ge as a function of the atomic volume normalized to Ω_{expt} (Ref. 31). The dashed line is the common tangent of the energy curves for the diamond phase and the β -tin phase ($c/a = 0.551$).
- Fig. 7 Contour plot of the (valence) charge density in the $(\bar{2}110)$ plane of the hexagonal diamond phase of Si at Ω_{expt} (conventions of Fig. 4).
- Fig. 8 Charge density contour plots of six phases of Si at $0.751 \Omega_{\text{expt}}$ (conventions of Fig. 4).
- Fig. 9 (a) Contour plot of the charge density of the bcc phase of Si at $0.751 \Omega_{\text{expt}}$ constructed from a superposition of pseudoatomic charge densities. (b) Contour plot of the difference between Figs. 8(d) and 9(a) (conventions of Fig. 4).
- Fig. 10 The ball-and-stick model for the diamond crystal structure. The dashed lines denote the cubic unit cells and the solid lines denote the tetragonal unit cell.
- Fig. 11 Total energy curves of the diamond phase and the β -tin phases with axial ratios (i) 0.552, (ii) 0.621, (iii) 0.488, and (iv) 0.458 as a function of the atomic volume normalized to Ω_{expt} . The dashed line is the common tangent of the energy curves for the diamond phase and the β -tin phase (i).
- Fig. 12 Individual energy contributions of the β -tin phase

of Si as a function of the axial ratio at a fixed atomic volume of $0.71 \Omega_{\text{expt}}$. (The contribution E'_{ec} has a constant 2.285 subtracted out.)

Fig. 13 Ewald constant of the β -tin phase as a function of axial ratio (c/a).

Fig. 14 Differences between various contributions to the total energy of the diamond phase and the β -tin phase ($c/a = 0.552$) of Si as a function of atomic volume (normalized to Ω_{expt}).

Fig. 15 Electronic structure of Si. The numbers refer to the conventional indices for symmetry group representations. Energies are measured from the valence band maximum (Γ_{25}).

Fig. 16 Electronic structure of Ge. Conventions of Fig. 15.

Fig. 17 Density of states of Si in units of state/eV-atom. Energies are measured from the valence band maximum.

Fig. 18 Density of states of Ge. Conventions of Fig. 17.

Fig. 19 Ab initio pseudopotential of Si generated²² using 1.35, 1.56, and 1.56 a.u. for γ_c values of s, p, and d components.

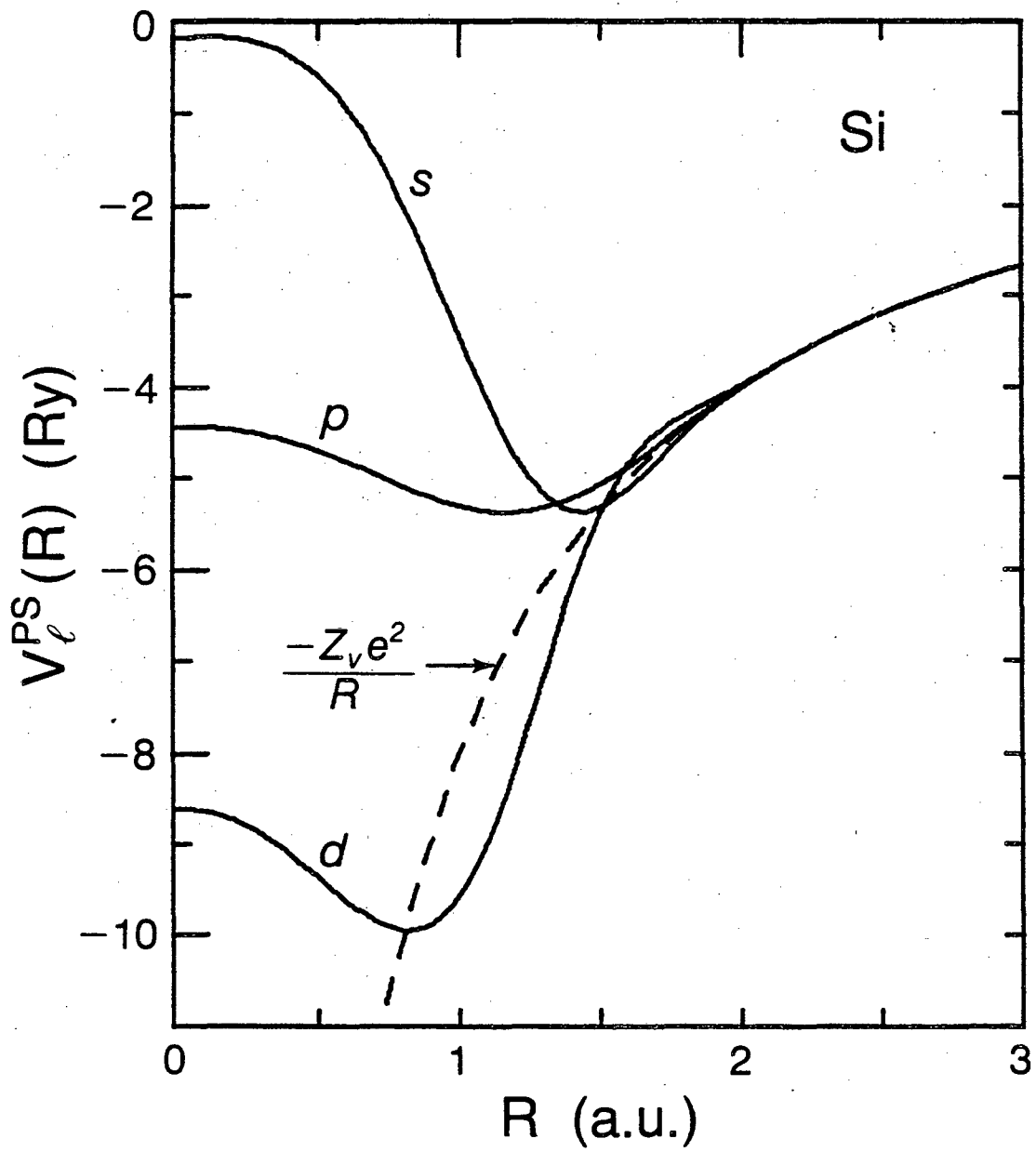


Fig. 1a

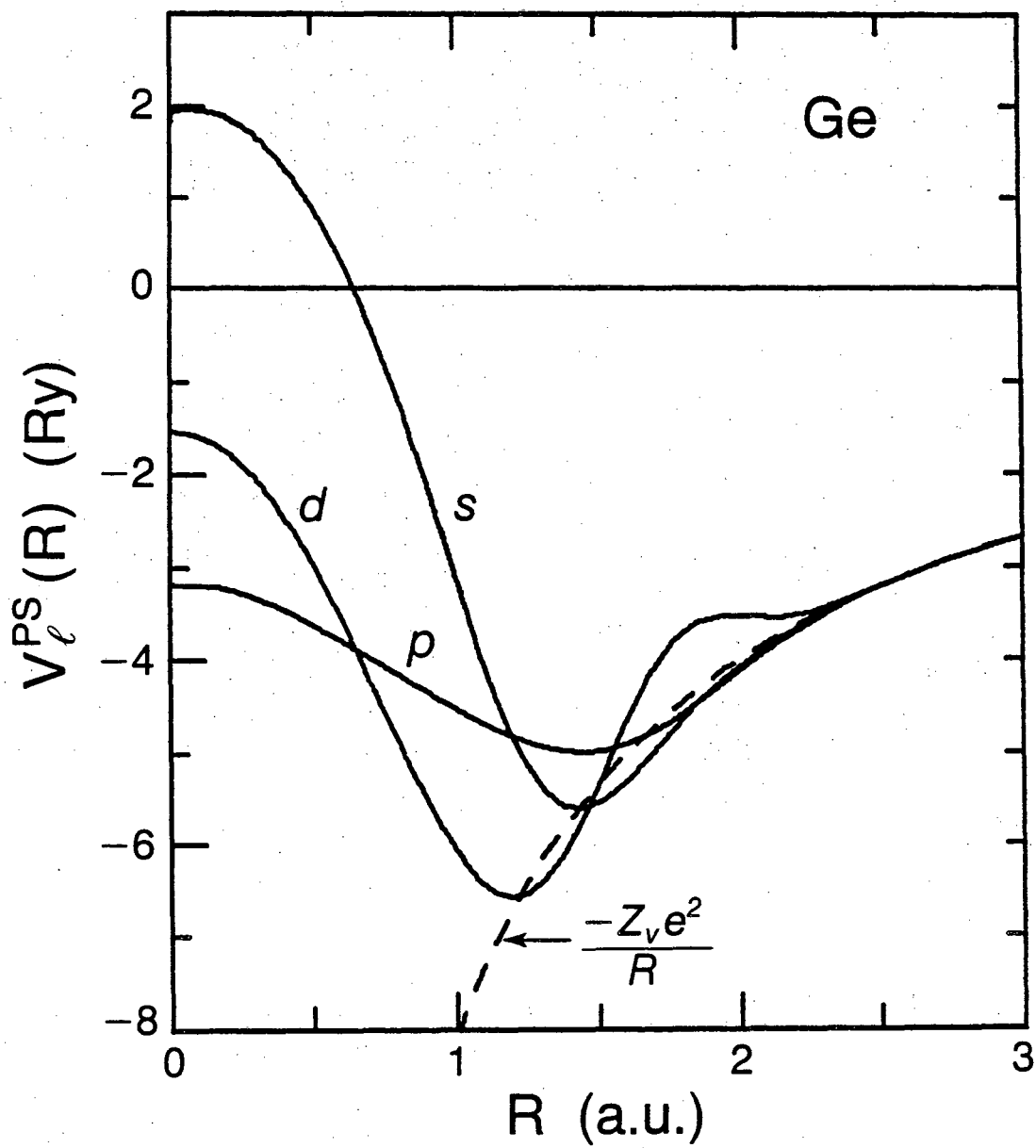


Fig. 1b

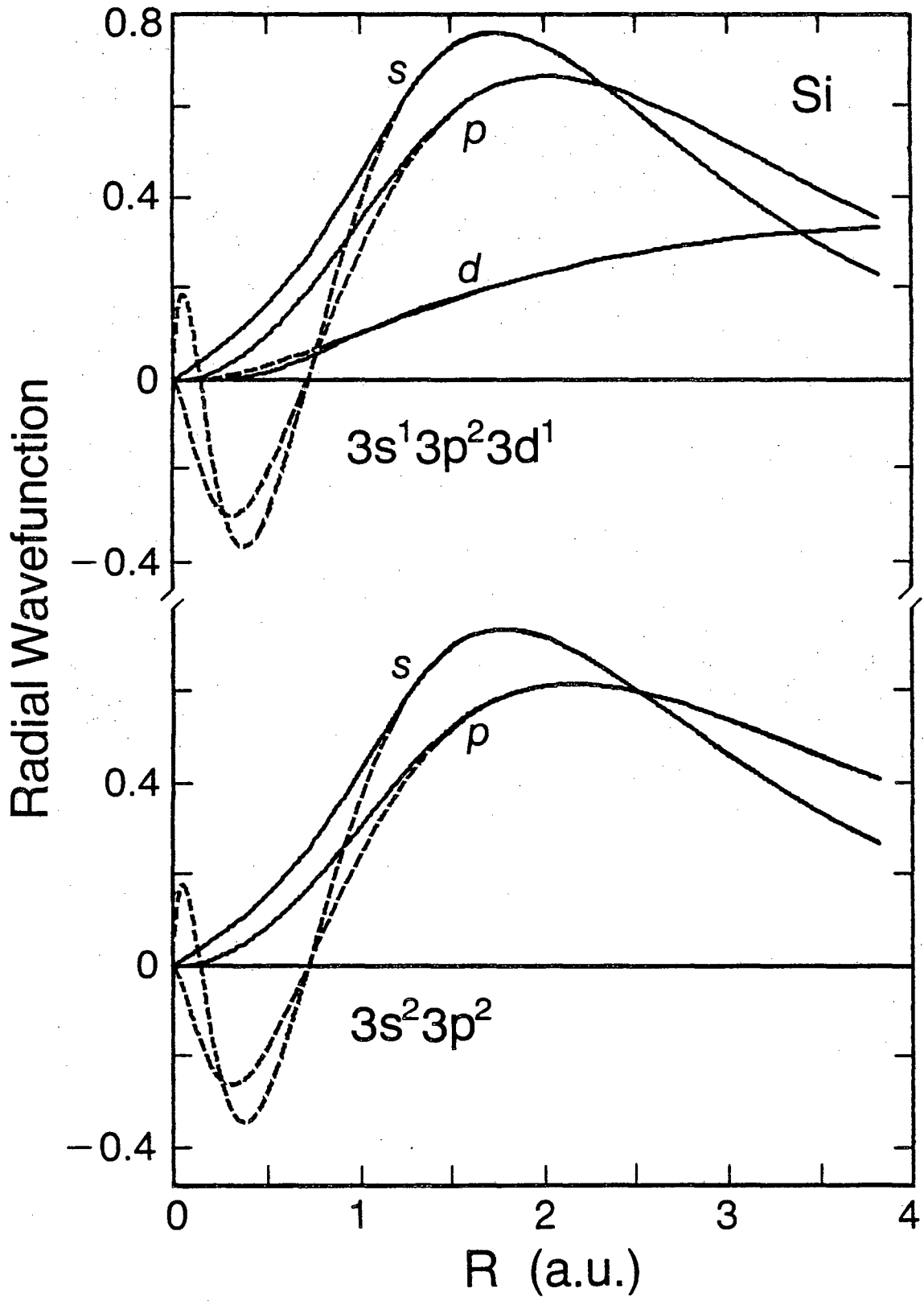


Fig. 2

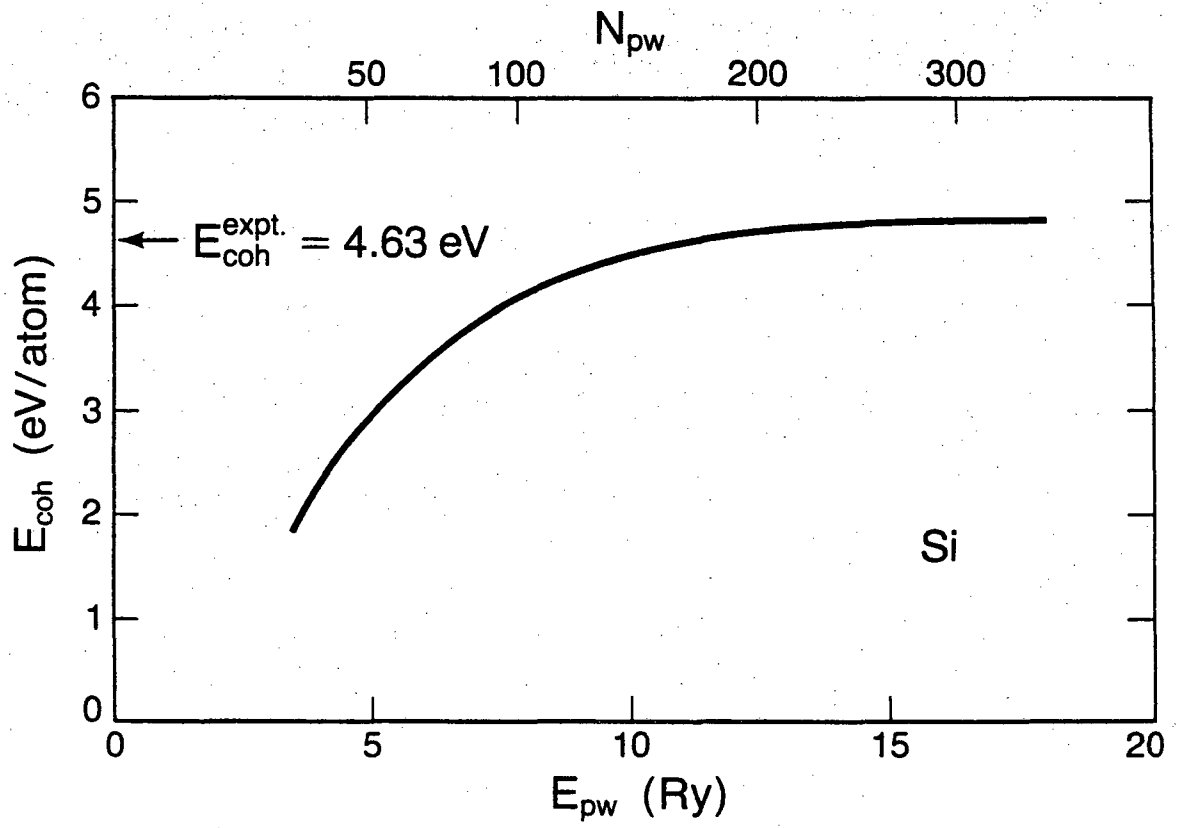


Fig. 3

Valence charge density (110 plane)

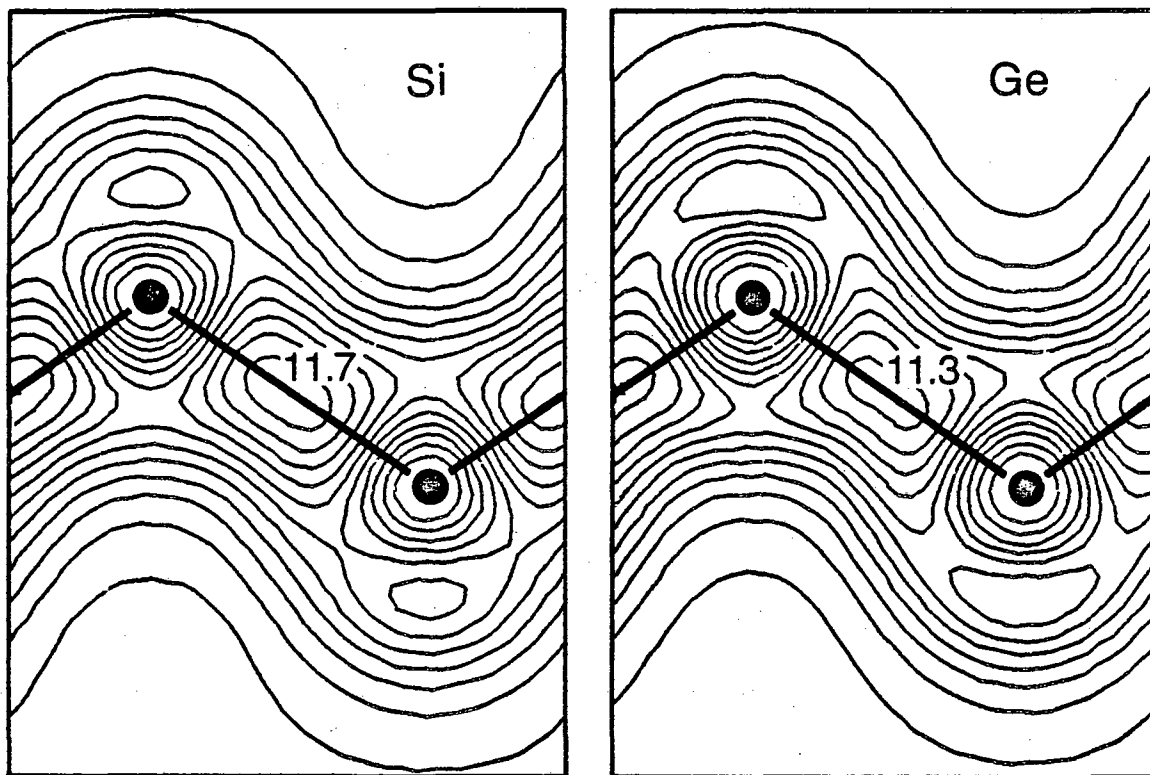


Fig. 4

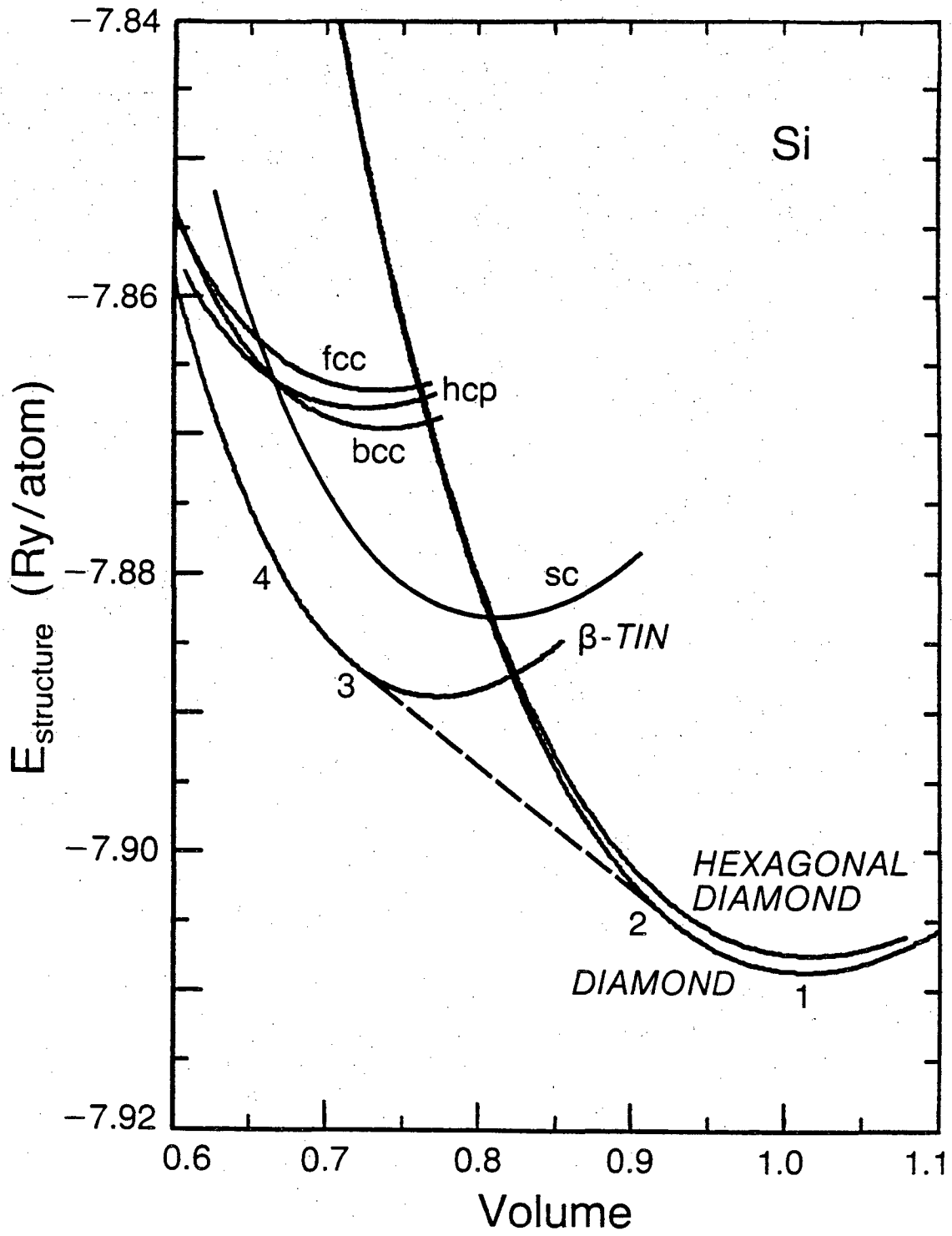


Fig. 5

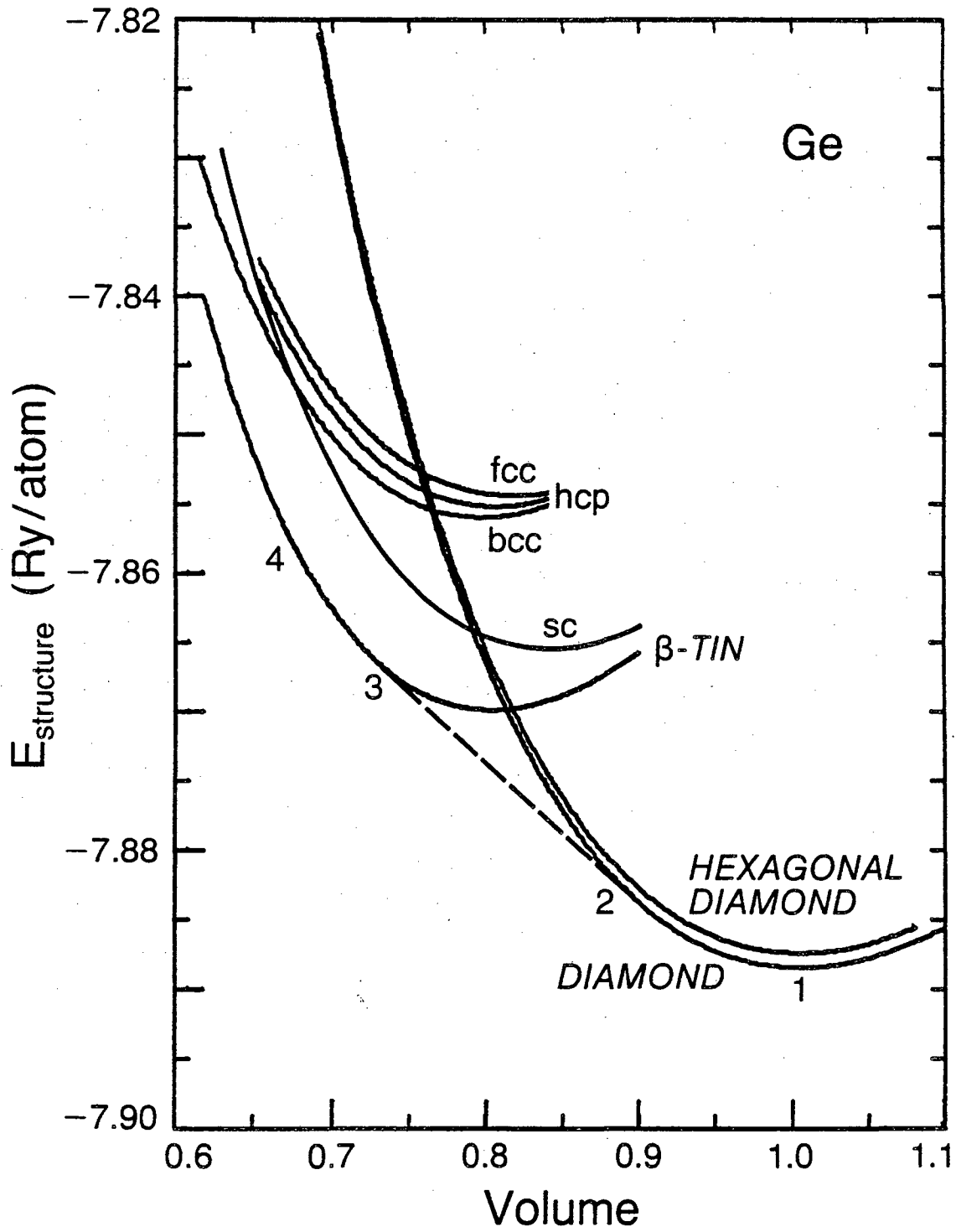


Fig. 6

Hexagonal diamond ($\bar{2}110$)

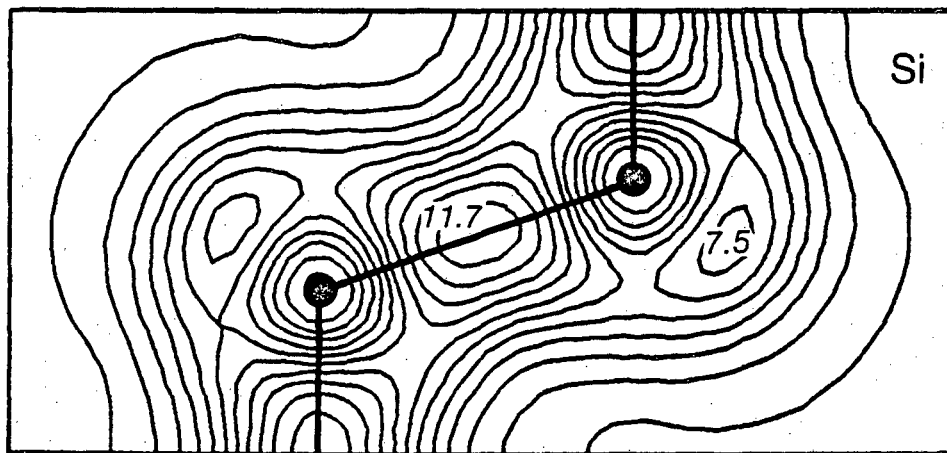


Fig. 7

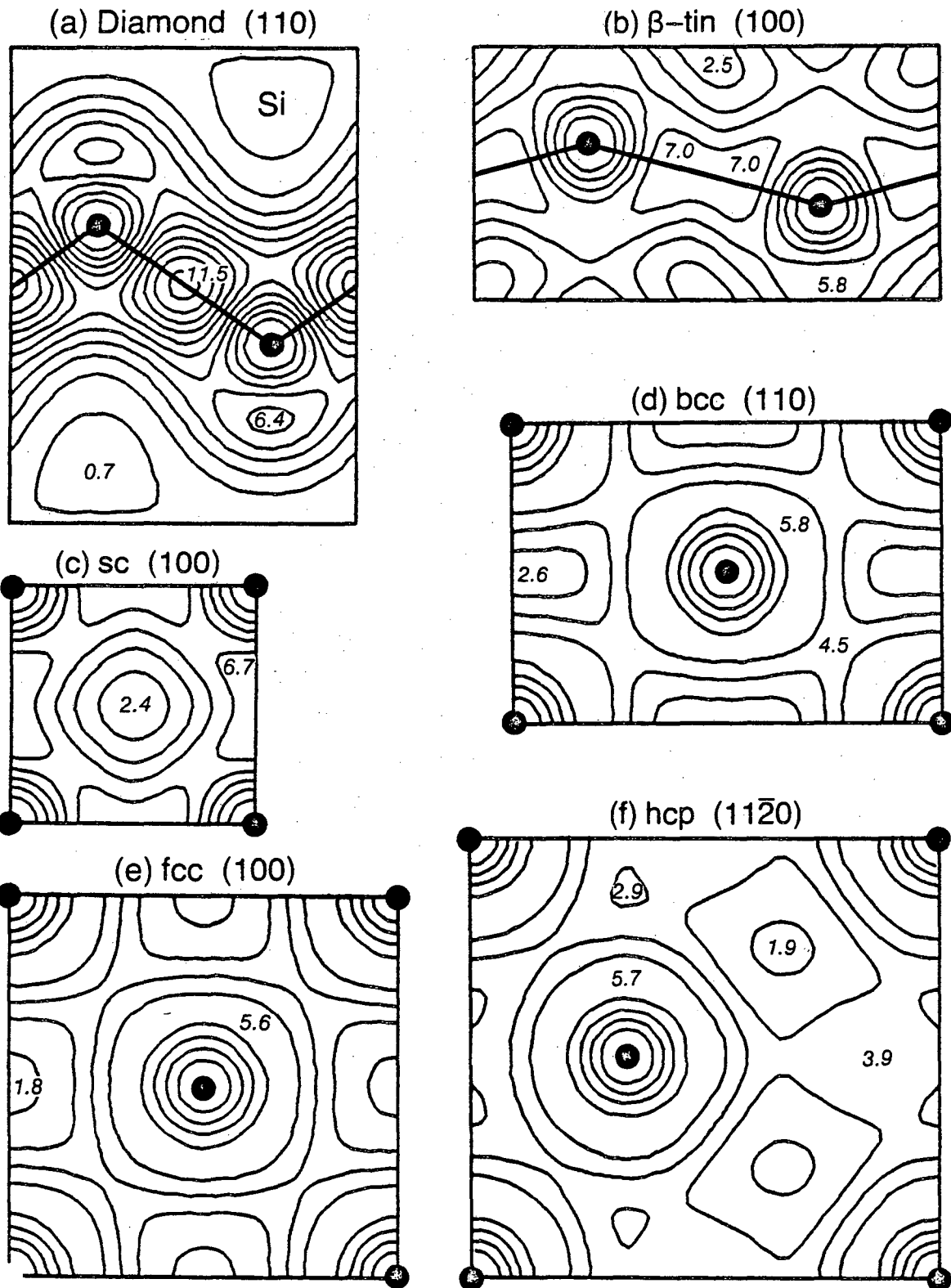


Fig. 8

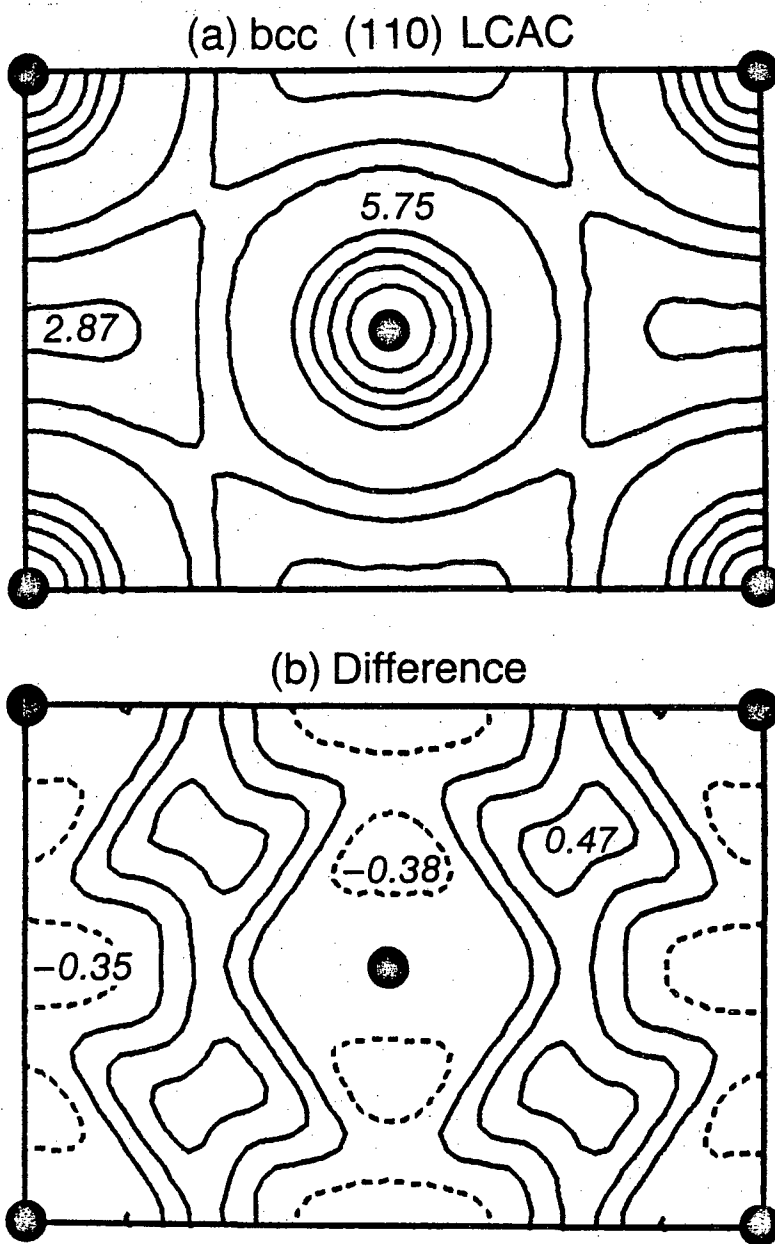


Fig. 9

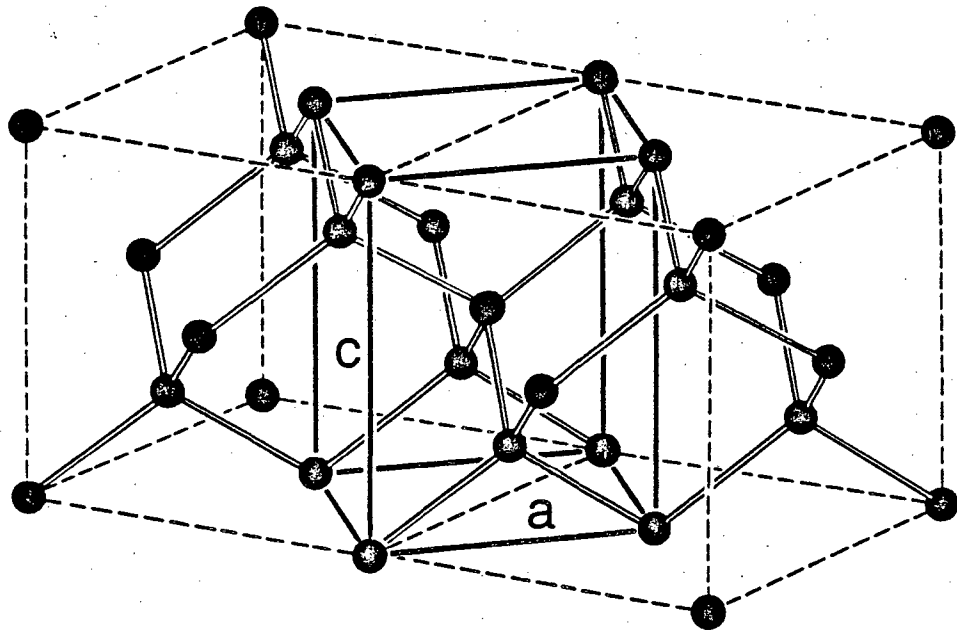


Fig. 10

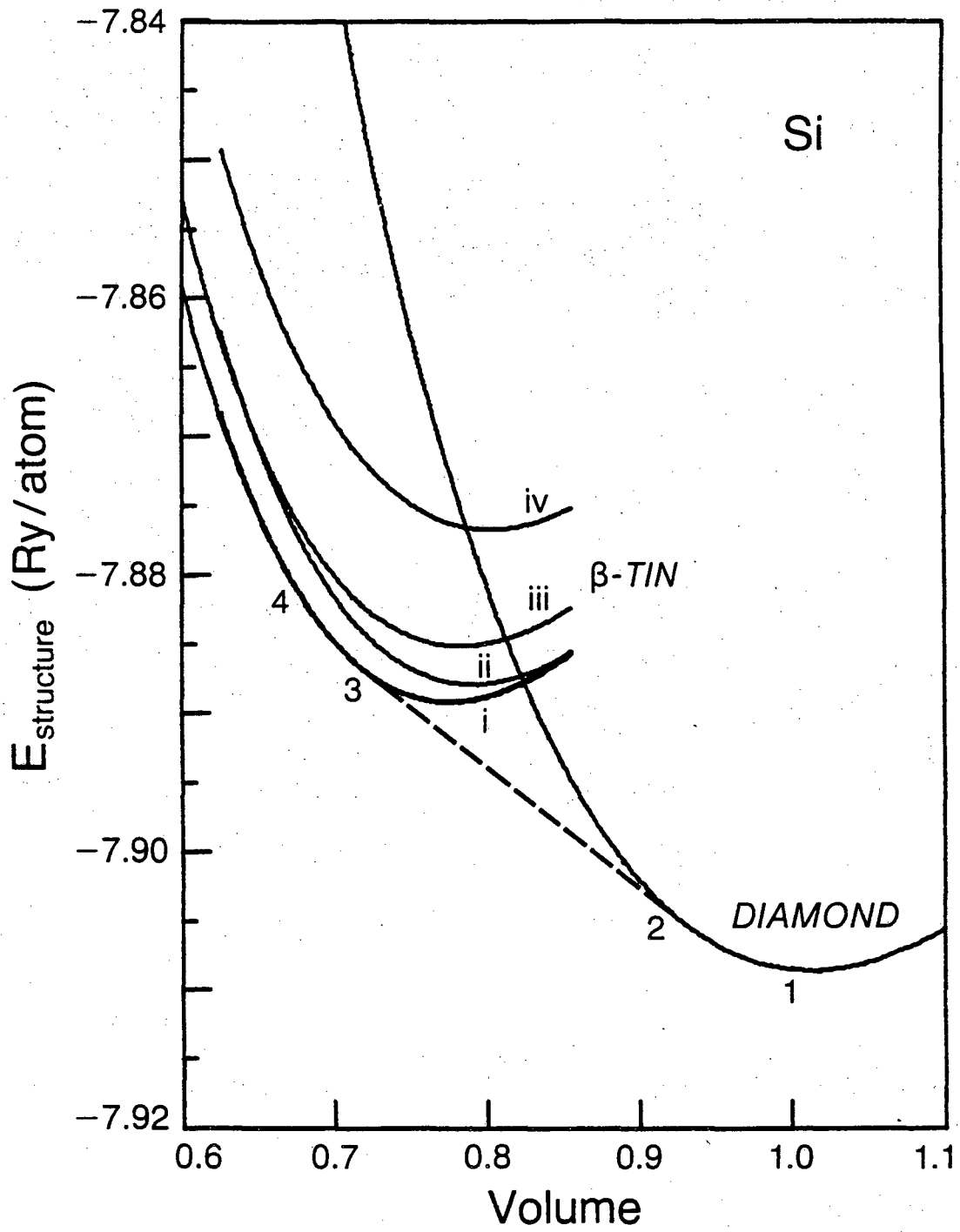


Fig. 11

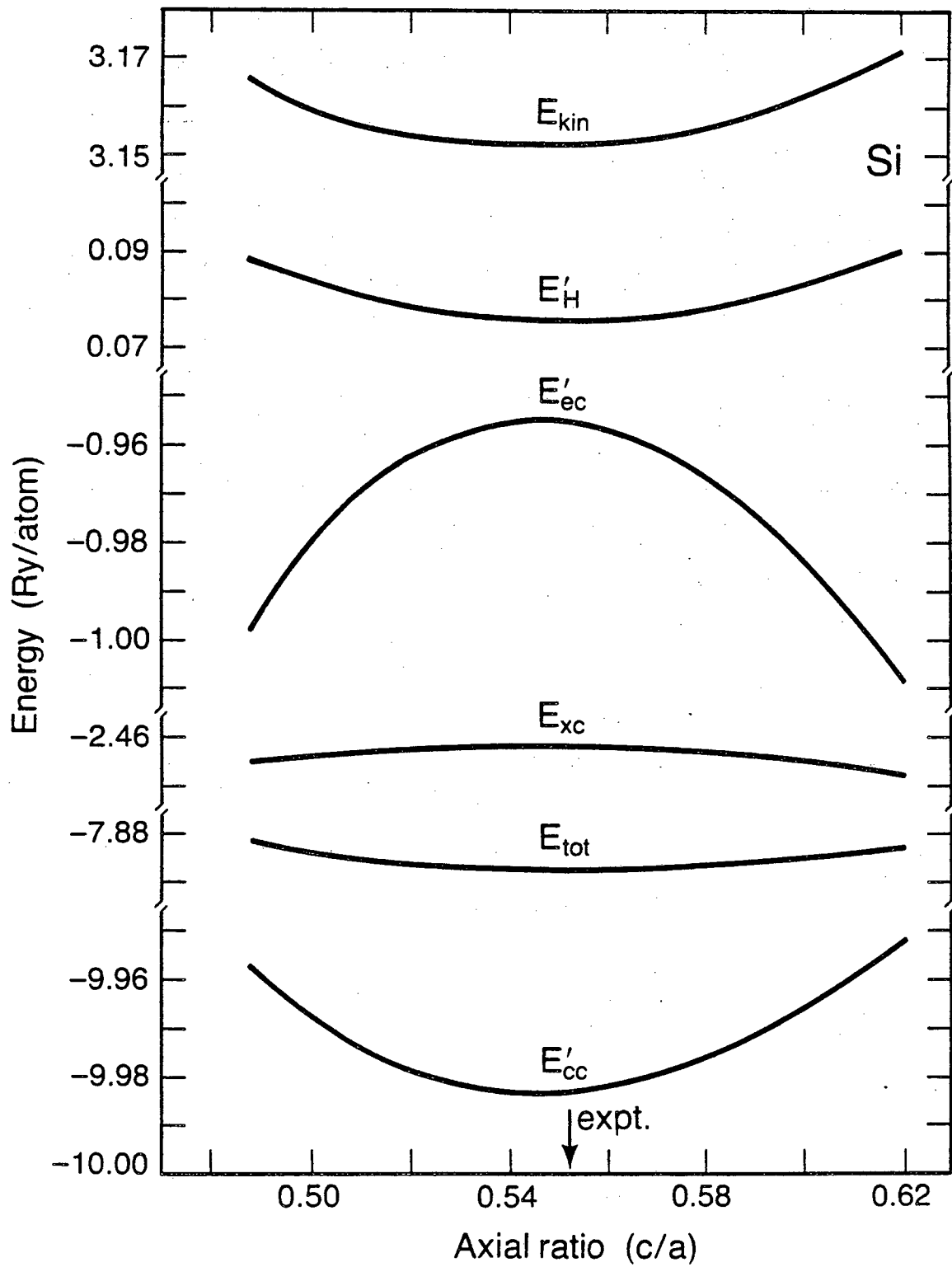


Fig. 12

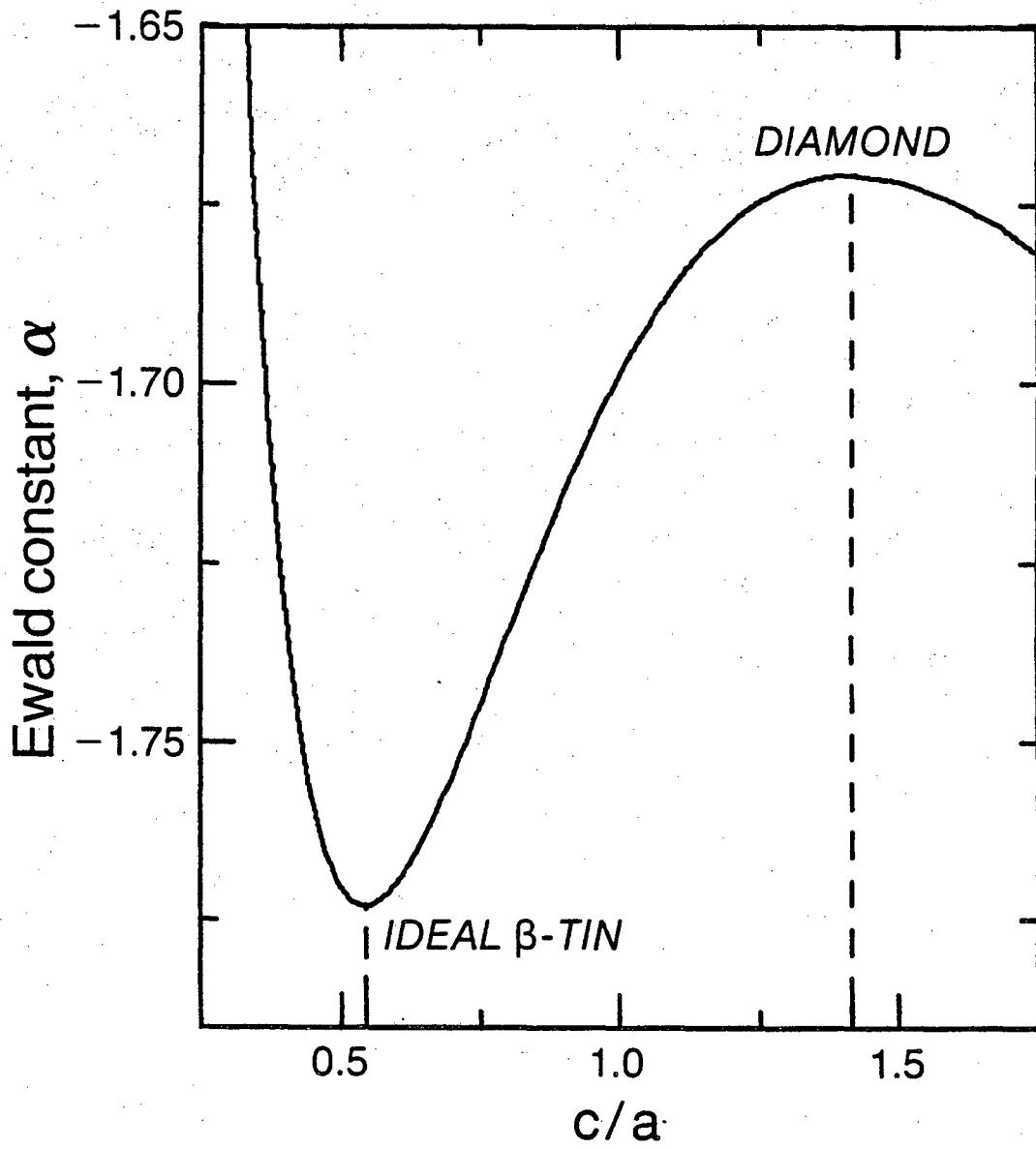


Fig. 13

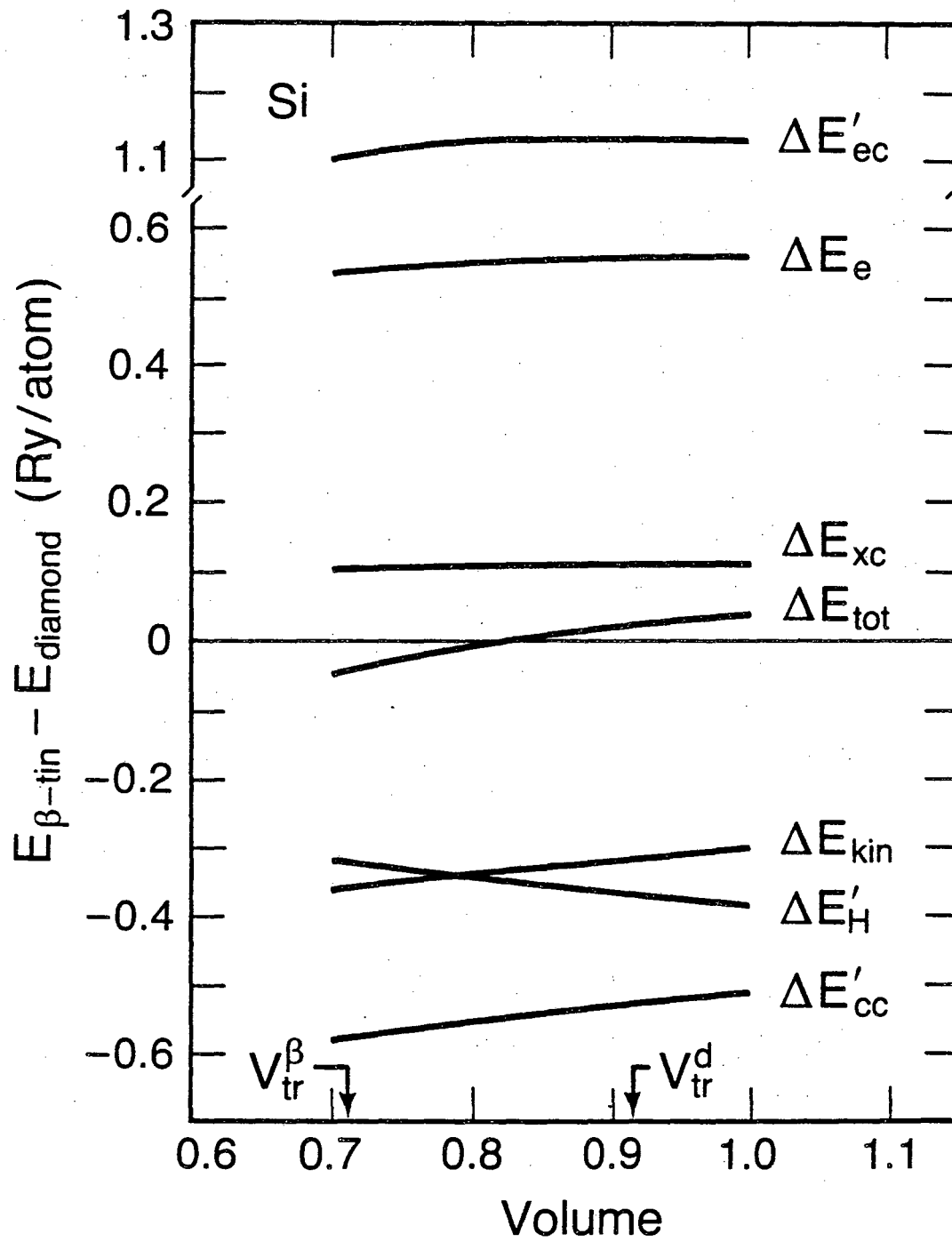


Fig. 14

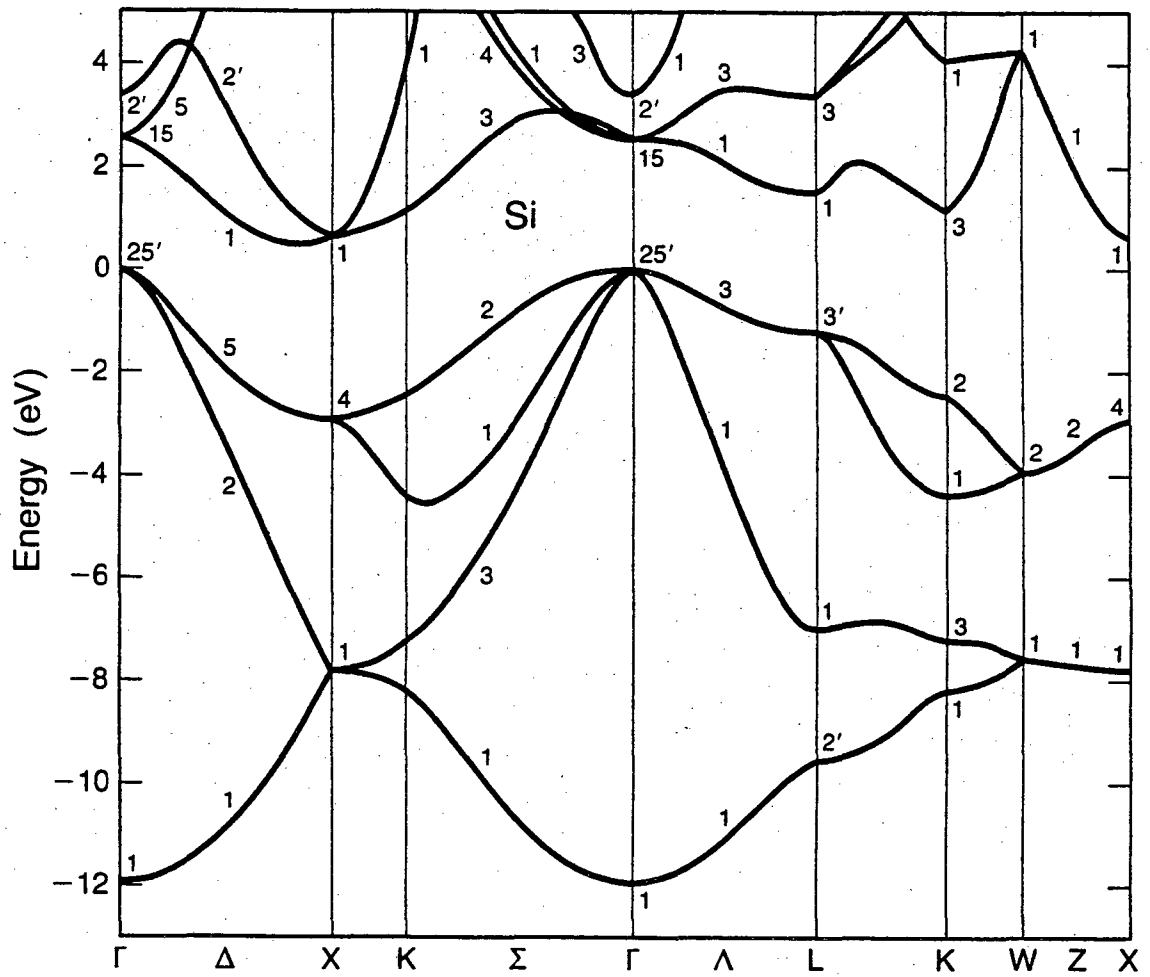


Fig. 15

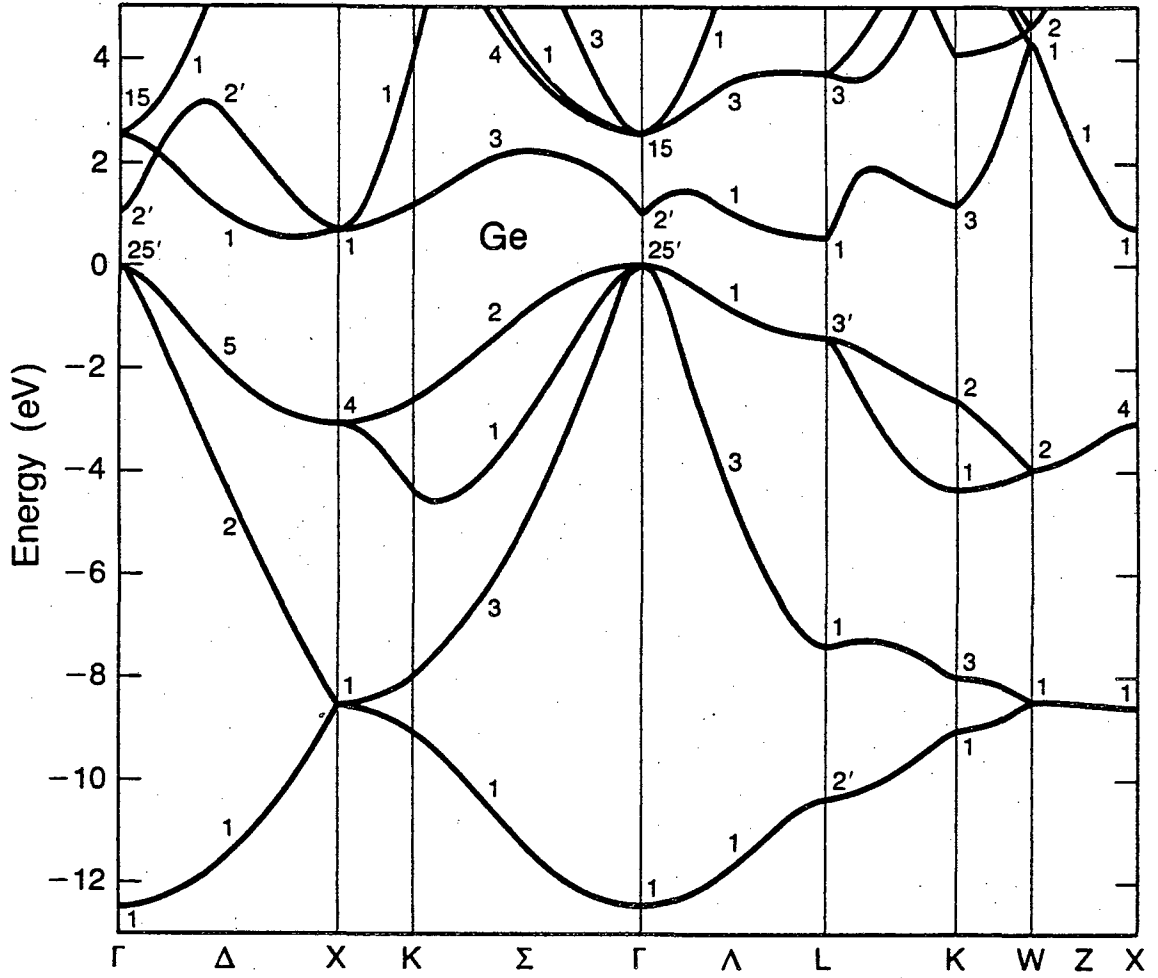


Fig. 16

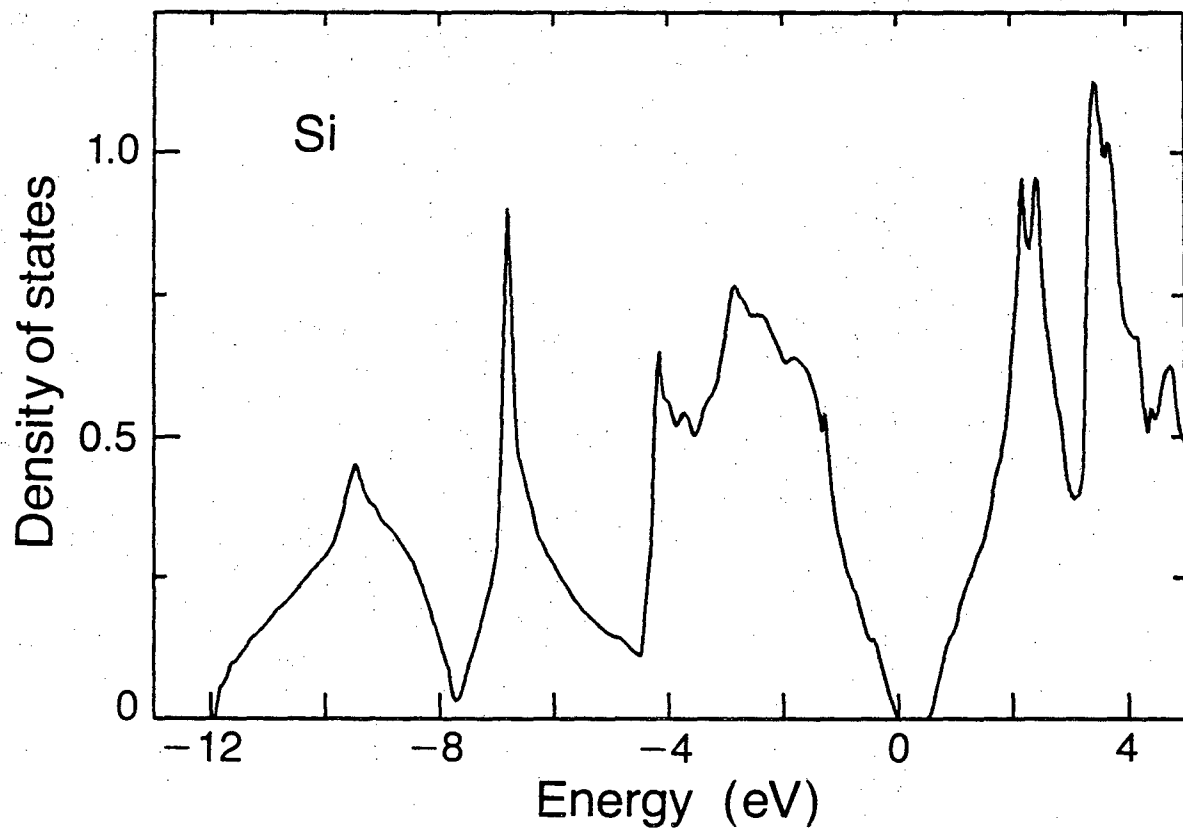


Fig. 17

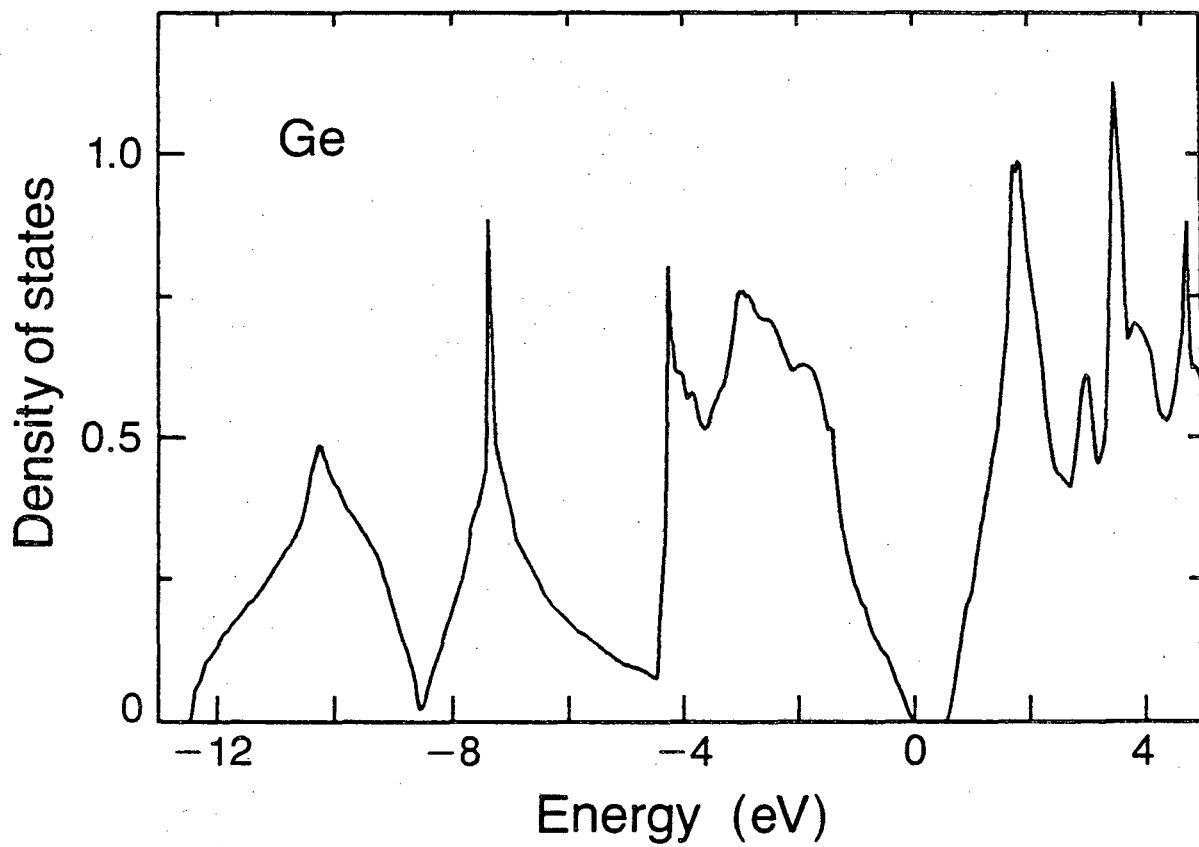


Fig. 18

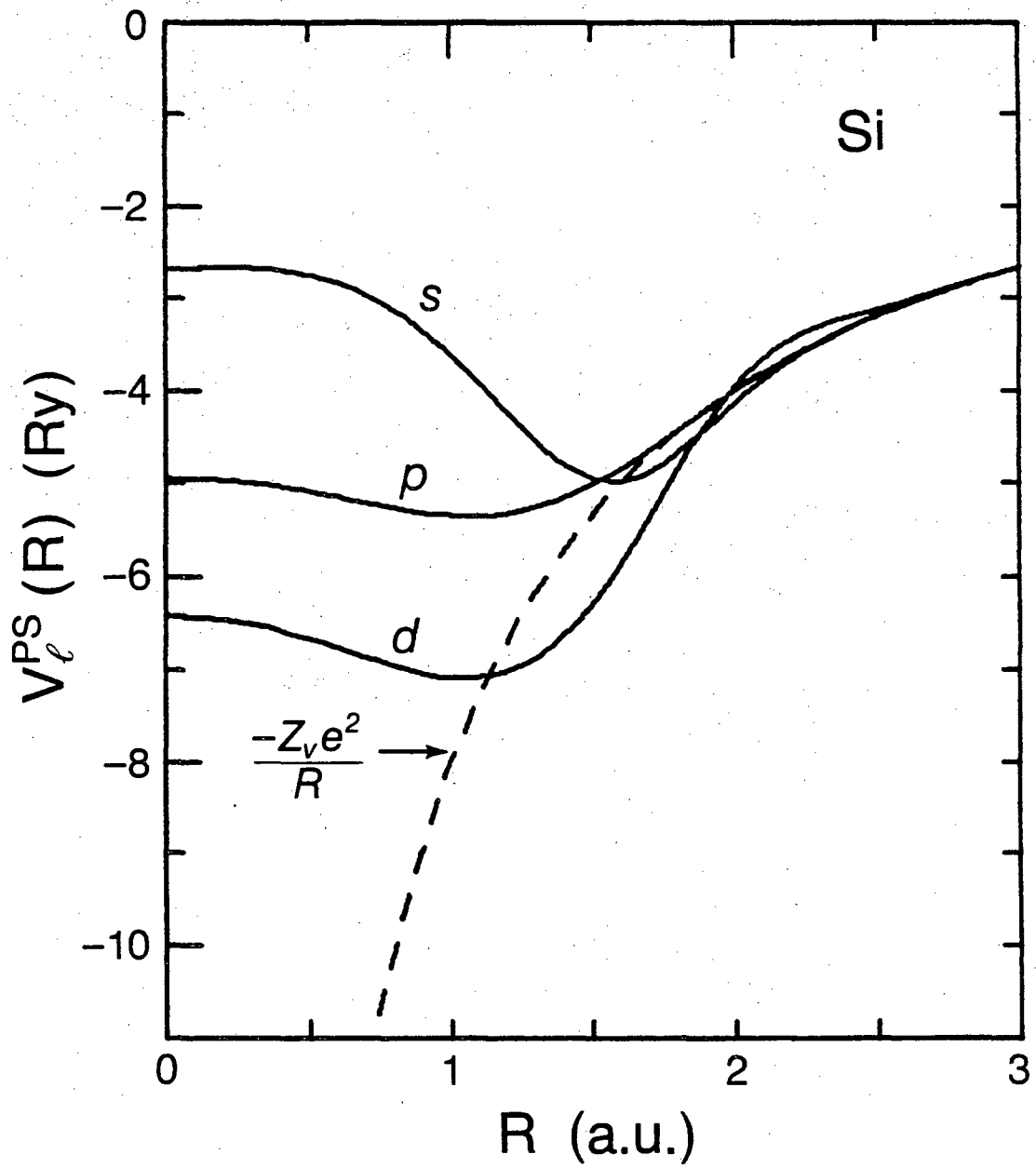


Fig. 19

This report was done with support from the Department of Energy. Any conclusions or opinions expressed in this report represent solely those of the author(s) and not necessarily those of The Regents of the University of California, the Lawrence Berkeley Laboratory or the Department of Energy.

Reference to a company or product name does not imply approval or recommendation of the product by the University of California or the U.S. Department of Energy to the exclusion of others that may be suitable.

TECHNICAL INFORMATION DEPARTMENT
LAWRENCE BERKELEY LABORATORY
UNIVERSITY OF CALIFORNIA
BERKELEY, CALIFORNIA 94720